Neurobiology of Disease

Downmodulation of Potassium Conductances Induces Epileptic Seizures in Cortical Network Models Via Multiple Synergistic Factors

Ernest C. Y. Ho (何鎮宇),[1] Adam J. H. Newton,[2] Eugenio Urdapilleta,[3] Salvador Dura-Bernal,[2,4] and Wilson Truccolo[1,5]
[1]Department of Neuroscience, Brown University, Providence, Rhode Island 02912, [2]Department of Physiology and Pharmacology, State University of New York (SUNY), Downstate Health Sciences University, Brooklyn, New York 11203, [3]Centro Atómico Bariloche and Instituto Balseiro, Consejo Nacional de Investigaciones Científicas y Técnicas (CONICET), Universidad Nacional de Cuyo, R8402AGP Bariloche, Río Negro, Argentina, [4]Center for Biomedical Imaging and Neuromodulation, Nathan S. Kline Institute for Psychiatric Research, Orangeburg, New York 10962, and [5]Carney Institute for Brain Science, Brown University, Providence, Rhode Island 02912

Voltage-gated potassium conductances g_K play a critical role not only in normal neural function, but also in many neurological disorders and related therapeutic interventions. In particular, in an important animal model of epileptic seizures, 4-aminopyridine (4-AP) administration is thought to induce seizures by reducing g_K in cortex and other brain areas. Interestingly, 4-AP has also been useful in the treatment of neurological disorders such as multiple sclerosis and spinal cord injury, where it is thought to improve action potential propagation in axonal fibers. Here, we examined g_K downmodulation in biophysical models of cortical networks that included different neuron types organized in layers, potassium diffusion in interstitial and larger extracellular spaces, and glial buffering. Our findings are fourfold. First, g_K downmodulation in pyramidal and fast-spiking inhibitory interneurons led to differential effects, making the latter much more likely to enter depolarization block. Second, both neuron types showed an increase in the duration and amplitude of action potentials, with more pronounced effects in pyramidal neurons. Third, a sufficiently strong g_K reduction dramatically increased network synchrony, resulting in seizure-like dynamics. Fourth, we hypothesized that broader action potentials were likely to not only improve their propagation, as in 4-AP therapeutic uses, but also to increase synaptic coupling. Notably, graded-synapses incorporating this effect further amplified network synchronization and seizure-like dynamics. Overall, our findings elucidate different effects that g_K downmodulation may have in cortical networks, explaining its potential role in both pathological neural dynamics and therapeutic applications.

Key words: **4-aminopyridine; focal epilepsy; ionic diffusion; network synchronization**

Significance Statement

The modulation of voltage-gated potassium-conductances g_K is thought to play an important role in epileptic seizures and therapeutic interventions in epilepsy, multiple sclerosis and spinal-cord injury. We show that g_K downmodulation can lead to a cascade of effects including changes in basal excitability, broadening of action potentials resulting in enhanced robustness to synaptic noise perturbations and strengthening of synaptic coupling; and differential effects in excitatory and fast-spiking inhibitory interneurons, promoting depolarization block in the latter under strong downmodulation. All these effects synergistically contribute to the emergence of seizure-like dynamics in the form of almost-periodic synchronized neuronal-population spiking in cortical networks. Under appropriate levels, g_K downmodulation can also have therapeutic effects by improving neuronal communication via the broadening of action potentials.

Received Oct. 9, 2023; revised Jan. 17, 2025; accepted Jan. 22, 2025.

Author contributions: E.C.Y.H. and W.T. designed research; E.C.Y.H. and W.T. performed research; E.C.Y.H., A.J.H.N., E.U., S.D-B., and W.T. contributed unpublished reagents/analytic tools; E.C.Y.H. and W.T. analyzed data; E.C.Y.H. and W.T. wrote the first draft of the paper; E.C.Y.H., A.N., E.U., S.D-B., and W.T. edited the paper; E.C.Y.H. and W.T. wrote the paper.

This research was supported by the National Institutes of Health (NIH), National Institute of Neurological Disorders and Stroke (NINDS), grant R01NS079533 (WT), and the Pablo J. Salame Goldman Sachs endowed Associate Professorship of Computational Neuroscience at Brown University (WT), and NIH NIBIB U24EB028998 (NetPyNE funding, SDB). Part of this research was conducted using computational resources and services at the Center for Computation and Visualization, Brown University, supported in part by the NIH grant S10 OD025181. We thank the editors and reviewers for their meticulous reading of the manuscript, and are appreciative of their valuable comments which improved the quality of this work.

The authors declare no competing financial interest.

Correspondence should be addressed to Wilson Truccolo at wilson_truccolo@brown.edu.

https://doi.org/10.1523/JNEUROSCI.1909-23.2025

Introduction

Excitability and spiking properties of neurons are dependent on the regulation of potassium concentrations by means of different ion channels and interactions with glial cells (Thier, 1986; Bean, 2007). Hence, potassium conductances (g_K) play a critical role not only in normal function but also in many neurological disorders and related therapeutic interventions. Abnormal potassium conductances and concentrations have been for decades hypothesized to play a fundamental role in seizure onset in many types of epilepsies (Smart et al., 1998; Köhling and Wolfart, 2016), and have been examined in many biophysical models (Kager et al., 2000; Somjen, 2002; Bazhenov et al., 2004; Fröhlich et al., 2008; Somjen et al., 2008; Cressman et al., 2009; Ullah et al., 2009; Fröhlich et al., 2010; Krishnan et al., 2013; Wei et al., 2014a,b; Ho and Truccolo, 2016; Gentiletti et al., 2022).

Modulation of g_K has also been an important mechanism underlying both animal models of seizures as well therapeutic interventions. Recently, an important proof of concept of the latter has been provided for the use of a gene therapy strategy based on closed-loop prevention of epileptic seizures by transiently driving the expression of potassium channels (Kv1.1) in neurons, thus downregulating excitability, only in response to periods of abnormal hyperactivity that would otherwise typically lead to seizures (Qiu et al., 2022).

A prominent example motivating our study is the use of the potassium-channel blocker 4-AP to induce focal seizures in animal models (Avoli et al., 1996; Žiburkus et al., 2006; Librizzi et al., 2017; Wenzel et al., 2017, 2019; Scalmani et al., 2023). 4-AP administration is thought to induce seizures by downmodulating g_K in cortex and other brain areas, thus decreasing outward potassium currents and increasing neuronal excitability (Bean, 2007; Myers et al., 2018). In contrast to low-voltage fast-activity seizures (Truccolo et al., 2011; Perucca et al., 2013; Truccolo et al., 2014; Wagner et al., 2015), 4-AP induced seizures typically evolve into sequences of spike-wave discharges in measured field potentials.

Interestingly, 4-AP has also been considered as an important alternative in the treatment of neurological disorders such as multiple sclerosis, spinal-cord injury, cerebellar ataxia and encephalopathy disorders (Sherratt et al., 1980; Bostock et al., 1981; Alviña and Khodakhah, 2010; Dietrich et al., 2021; Hedrich et al., 2021; Paredes-Cruz et al., 2022). In the former two, 4-AP administration appears to prolong and facilitate action potential propagation in axonal fibers. The effect is thought to be mediated by the broadening, i.e., an increase in the temporal width and amplitude, of action potentials. Furthermore, this broadening effect is hypothesized to result from the 4-AP reduction in neuronal g_K (Locke and Nerbonne, 1997a,b; Yuan et al., 2005).

Modulation of g_K conductances can lead to very complex cascade effects, making the understanding of the emergent dynamics in neuronal networks very challenging. Here, we provide a unifying perspective on the multiple synergistic effects that g_K downmodulation might have in both normal and abnormal neural dynamics. We focus on conductances of voltage-gated, specifically delayed rectifier, potassium channels. We developed biophysical models of neocortical networks that include excitatory pyramidal and fast-spiking (FS) inhibitory interneurons spatially organized in layers 2–3 and 5–6, potassium diffusion in interstitial and larger extracellular spaces, and glial potassium-buffering. Furthermore, we hypothesize that broader action potentials are likely to not only improve their propagation, as in 4-AP administration for MS, but more important to our context, to also increase synaptic coupling. The arrival of action potentials with longer durations and higher amplitudes at pre-synaptic sites is expected to increase Ca^{2+} inflow, thus increasing the number or the likelihood of synaptic vesicle release, and strengthening synaptic coupling (Barish et al., 1996; Wheeler et al., 1996; Scarnati et al., 2020). To examine these hypothesized synaptic gaining effects we implemented graded-synapses in the neuronal coupling in the modeled cortical networks. Overall, we systematically examined how g_K downmodulation differentially affected depolarization block in pyramidal and inhibitory interneurons, neuronal network synchrony and induction of abnormal activity patterns akin to seizures.

Materials and Methods

Single neuron model

Biophysical models of single neurons of various levels of complexity have been applied to epilepsy studies in the past, including neuronal models with a large number of compartments and ionic currents as in the work by Traub and colleagues (Traub et al., 2005). Here, given the required large number of stochastic simulations to systematically probe the effects of the variations in many different parameters and g_K downmodulation scenarios, we focused on smaller models. In particular, we used the same type and number of conductances as in the study by Timofeev and colleagues (Timofeev et al., 2000). In addition, here we do not address dendritic and axonal ectopic events (Traub et al., 1995). Instead, we focused on somatic and synaptic mechanisms using single compartment models to represent pyramidal neurons and FS inhibitory interneurons (Wang and Buzsáki, 1996; Skinner, 2006; Anderson et al., 2007; Ho and Truccolo, 2016). The model can be expressed by a set of ordinary differential equations of membrane potential V as follows:

$$C \times \frac{dV}{dt} = I_{\text{int}}(t) + I_{\text{ext}}(t) - \frac{I_{\text{Kpump}}(t)}{2}, \tag{1}$$

where C is the specific capacitance which we assume to have the value of 1 μF/cm^2.

The currents I_{int}, I_{ext}, and I_{Kpump} are described in the next sections. Table 1 lists the parameters and corresponding values used in the simulations of single neuron and network models in this study.

Ionic currents. $I_{\text{int}}(t)$ of Equation 1 represents the intrinsic currents of the neuron and has the following general form:

$$\begin{aligned} I_{\text{int}}(t) = &-I_{\text{Na}}(t) - I_{\text{Nap}}(t) - I_K(t) - I_{\text{Km}}(t) - I_{\text{Ca}}(t) - I_{L\,|\,\text{Na}}(t) \\ &- I_{L\,|\,K}(t) - I_{L\,|\,\text{Cl}}(t) - I_{\text{KCa}}(t). \end{aligned} \tag{2}$$

The above Equation 2 represents the (negative of) the sum of voltage-gated sodium, persistent sodium, voltage-gated potassium, M-type potassium, calcium, sodium leak, potassium leak, chloride leak and calcium-mediated potassium currents, respectively.

The voltage-gated sodium, persistent sodium, voltage-gated potassium, M-type potassium, calcium and the various leak currents have the following standard form:

$$I_{\text{Na}}(t) = g_{\text{Na}} \times m_\infty^3 \times h \times (V - E_{\text{Na}}), \tag{3}$$

$$I_{\text{Nap}}(t) = g_{\text{NaP}} \times j \times (V - E_{\text{Na}}), \tag{4}$$

$$I_K(t) = g_K \times n^4 \times \left(V - E_K\left([K^+]_o\right)\right), \tag{5}$$

$$I_{\text{Km}}(t) = g_{\text{Km}} \times l \times (V - E_K), \tag{6}$$

$$I_{\text{Ca}}(t) = g_{\text{Ca}} \times \frac{(V - E_{\text{Ca}})}{1 + \exp\left(-\dfrac{V + 25\,\text{mV}}{2.5\,\text{mV}}\right)}, \tag{7}$$

$$I_{L\,|\,\text{Na}}(t) = g_{L\,|\,\text{Na}} \times (V - E_{\text{Na}}), \tag{8}$$

$$I_{L\,|\,\text{Cl}}(t) = g_{L\,|\,\text{Cl}} \times (V - E_{\text{Cl}}), \tag{9}$$

$$I_{L\,|\,K}(t) = g_{L\,|\,K} \times \left(V - E_K\left([K^+]_o\right)\right). \tag{10}$$

Table 1. Intrinsic, glial and ionic parameters used in single neuron and network simulations, unless otherwise specified

			Value	
Parameter	Description	Units	Pyramidals	Interneurons
C	Specific neuron membrane capacitance	μF/cm^2	1	
R_{soma}	Soma radius (Fig. 1)	μm	22.5	27.5
L_{soma}	Soma length	μm	41.38	
d_{FHS}	Depth of interstitial space (Fig. 1, Eq. 25)	μm	0.2	
g_{Na}	Sodium conductance	mS/cm^2	35	
g_{NaP}	Persistent sodium conductance	mS/cm^2	0.2	0
g_{Km}	M-type potassium current conductance	mS/cm^2	0.02	0
$g_{L\mid K}$	Potassium leak conductance	mS/cm^2	0.035	
$g_{L\mid \text{Cl}}$	Chloride leak conductance	mS/cm^2	0.15	0.1
$g_{L\mid \text{Na}}$	Sodium leak conductance	mS/cm^2	0.025	
g_{Ca}	Calcium conductance	mS/cm^2	0.1	0.03
E_{Cl}	Chloride reversal potential	mV	−74	
E_{Na}	Sodium reversal potential	mV	70	
E_{Ca}	Calcium reversal potential	mV	120	
$[K^+]_i$	Intracellular potassium concentration (single neuron simulations)	mM	133	
I_{Kmax}	Maximal potassium pump current	μA/cm^2	7	
$[K^+]_{o(eq)}$	Equilibrium interstitial potassium concentration of I_{Kpump}	mM	3	
$[B]_{\max}$	Maximal glial free buffer concentration (Equation set 19)	mM	500	
k_b	Backward glial unbinding rate (Equation 18)	ms^{-1}	0.0008	
$[K^+]_{o(th)}$	Threshold interstitial potassium concentration of glial buffer (Equation set 19)	mM	15	
θ	See Equation set 19	mM	−1.15	
g_{KCa}	Ca^{2+}-activated potassium conductance	mS/cm^2	9	0
g_K	Potassium conductance	mS/cm^2	variable	variable
I_{ext}	External applied current to model neurons	μA/cm^2	variable	variable

A "variable" label on the value column denotes that the parameter is dependent on specific simulations. Please refer to the main text for specific values.

where g_{Na}, g_{Nap}, g_K, g_{Km}, g_{Ca} and $g_{L\mid\{\text{Na,Cl},K\}}$ are respectively the sodium, persistent sodium, potassium, M-type potassium, calcium and various ionic leak conductances, while $E_{\{\text{Na,Cl},K,\text{Ca}\}}$ are the sodium, chloride, potassium and calcium reversal potentials, respectively. E_K is a function of the variable $[K^+]_o$, which is the potassium concentration in the interstitial or Frankenhaeuser-Hodgkin space (Frankenhaeuser and Hodgkin, 1956; Beswick-Jones et al., 2023, Fig. 1*A*). E_K has the following form:

$$E_K = 26.64\,\text{mV} \times \log_e\left(\frac{[K^+]_o}{[K^+]_i}\right), \tag{11}$$

where $[K^+]_i$ indicates intracellular potassium concentration.

Each of the gating variables h, n, j and l obeys the set of differential equations below:

$$\frac{dX}{dt} = 5\,\text{ms}^{-1} \times (\alpha_X \times (1-X) - \beta_X \times X), \tag{12}$$

where X can be h, n, j or l, with

$$\begin{aligned}
\alpha_h(V) &= 0.07 \times \exp\left(-\tfrac{V+58\,\text{mV}}{20\,\text{mV}}\right),\\
\beta_h(V) &= \frac{1}{\exp(-0.1\,\text{mV}^{-1} \times (V+28\,\text{mV}))+1},\\
\alpha_n(V) &= -\frac{0.01\,\text{mV}^{-1} \times (V+34\,\text{mV})}{\exp(-0.1\text{mV}^{-1} \times (V+34\,\text{mV}))-1},\\
\beta_n(V) &= 0.125 \times \exp\left(-\frac{V+44\,\text{mV}}{80\,\text{mV}}\right),\\
\alpha_j(V) &= \frac{1}{1+\exp\left(-0.2\text{mV}^{-1} \times (V+42\,\text{mV})\right)},\\
\beta_j(V) &= 1-\alpha_j(V),\\
\alpha_l(V) &= -\frac{0.00058\,\text{mV}^{-1} \times (V+30\,\text{mV})}{\exp\left(-0.11\,\text{mV}^{-1} \times (V+30\,\text{mV})\right)-1},\\
\beta_l(V) &= \frac{0.00058\,\text{mV}^{-1} \times (V+30\,\text{mV})}{\exp\left(0.11\,\text{mV}^{-1} \times (V+30\,\text{mV})\right)-1}.
\end{aligned} \tag{13}$$

while the "fast" activation variable of I_{Na} has the form:

$$\begin{aligned}
m_\infty &= \frac{\alpha_m}{\alpha_m+\beta_m},\\
\alpha_m(V) &= \frac{-0.1\,\text{mV}^{-1} \times (V+35\,\text{mV})}{\exp\left(-0.1\text{mV}^{-1} \times (V+35\,\text{mV})\right)-1},\\
\beta_m(V) &= 4 \times \exp\left(-\frac{V+60\,\text{mV}}{18\,\text{mV}}\right).
\end{aligned} \tag{14}$$

Spike frequency adaptation of the neurons is provided by the calcium-mediated potassium current (I_{KCa}), which has the following form:

$$I_{\text{KCa}} = g_{\text{KCa}} \times (V-E_K) \times \frac{[\text{Ca}^{2+}]_i}{1\,\text{mM}+[\text{Ca}^{2+}]_i}, \tag{15}$$

where g_{KCa} and $[\text{Ca}^{2+}]_i$ are respectively the conductance for the current and the intracellular calcium ion concentration. The $[\text{Ca}^{2+}]_i$ dynamics are given by the following differential equation (Cressman et al., 2009; Ullah et al., 2009):

$$\frac{d[\text{Ca}^{2+}]_i}{dt} = -\frac{0.002\,\text{mol}}{\text{cm}\cdot\text{mC}} \times I_{\text{Ca}} - \frac{[\text{Ca}^{2+}]_i}{80\,\text{ms}}. \tag{16}$$

In the above setup for ionic currents we have made two main choices. First, we note that while working with simplified single-compartment models, variations in the calcium-mediated potassium conductance parameter g_{KCa} are central to the differential spiking dynamics in pyramidal vs. FS inhibitory interneurons. For comparison, in pyramidal neurons this conductance is the main mechanism for the generation of after-spike hyperpolarization on time scales of hundreds of milliseconds. It is also the main mechanism contributing to the almost periodic spiking at 2–3 Hz by these model neurons during seizures. On the other hand, in FS inhibitory interneurons, this g_{KCa} conductance tends to be very low, i.e., close to zero, thus allowing much higher firing rates. Therefore, here we followed the Wang and Buzsáki (1996) model and set $g_{\text{KCa}} = 0\,\text{mS/cm}^2$ in FS inhibitory interneurons.

Second, we emphasize that the focus of this study is not on the sensitivity of different voltage gated potassium channels to 4-AP, but rather on the more general effects of downmodulation of potassium channels on the spiking dynamics of single neurons and neuronal networks. Electrophysiologically, Kv3 type channels generally have a higher activation threshold than Kv1 channels (Kaczmarek and Zhang, 2017). In addition, while Kv1 are present on axonal initial segments of parvalbumin-positive neurons, Kv3 channels are present in the soma and highly expressed in axon terminals, facilitating fast GABA release at synaptic sites (Hijazi et al., 2023). However, despite these differences, both Kv1 and Kv3 channel families share the common mechanism of enhancing repolarization via facilitation of the effluxes of intracellular potassium ions to the interstitial space. The single-compartment models adopted here preserve the effects of this generic repolarization process, regardless of the specific location of Kv1 and Kv3 channels, i.e., somatic vs. presynaptic terminals. Furthermore, both channel types are selectively blocked by 4-AP, and their blockage contributes to depolarization block and AP broadening (Lien and Jonas, 2003; Kaczmarek and Zhang, 2017).

Consequently, the overall effects on neurons upon downmodulation of these channels (e.g., broadening of APs and corresponding synaptic effects at axonal terminals, and promotion of depolarization block in FS interneurons, to be examined in the Results section) are expected to be similar in our simulations whether we incorporate specific Kv1 and Kv3 kinetics or not. Therefore, we think that the use of more generic single-neuron models such as those in Wang and Buzsáki (1996) is sufficient for our purpose.

Glial and potassium dynamics. There are two major interstitial potassium regulation mechanisms at the single neuron level. First, the Na^+/K^+ transmembrane exchange pump moves two K^+ ions into the intracellular region for every 3 Na^+ ions going out to the interstitial region. The action of the pump on potassium ions has the following form:

$$I_{\text{Kpump}} = \frac{I_{\text{Kmax}}}{\left(1 + \frac{[K^+]_{o(eq)}}{[K^+]_o}\right)^2}, \tag{17}$$

where the parameter $[K^+]_{o(eq)}$ denotes the equilibrium interstitial potassium concentration for the pump.

The ion exchange process represented by Equation 17 results in a net flow of one cation from the intracellular region to the interstitial space for every two K^+ ions flowing into the intracellular region. Hence, there is an extra $\frac{I_{\text{Kpump}}}{2}$ being subtracted from the RHS of Equation 1 to account for the net Na^+/K^+ transmembrane exchange pump current in and out of the intracellular region (Buchin et al., 2016).

Second, the nearby glial cells also regulate interstitial potassium by means of a buffering mechanism. The glial buffering mechanism can be modelled as a chemical reaction that reversibly converts interstitial potassium to a bind substance (Kager et al., 2000), specified as follows:

$$K^+{}_o + B \underset{k_b}{\overset{k_f}{\rightleftharpoons}} \text{KB}, \tag{18}$$

where $K^+{}_o$ and B represent the interstitial potassium ions and the free buffer in the glia, respectively, and k_b and k_f denote the forward and backward glial binding rates, respectively. The first order dynamics of Equation 18 can be written as the set of differential equations below:

$$\begin{aligned} \frac{\partial [K^+]_o}{\partial t}\Big|_{\text{glia}} &= k_b \times \frac{[B]_{\max} - [B]}{1.1} - k_f \times [K^+]_o \times [B], \\ \frac{\partial [B]}{\partial t} &= k_b \times ([B]_{\max} - [B]) - k_f \times [K^+]_o \times [B], \\ k_f &= \frac{k_b / 1\,\text{mM}}{1 + \exp\left(\frac{[K^+]_o - [K^+]_{o(th)}}{\theta}\right)}, \end{aligned} \tag{19}$$

where $[K^+]_{o(th)}$ denotes the threshold for the interstitial potassium concentration of glial buffer (Table 1).

Total $[K^+]_o$ derivative. Accounting for every potassium current leads to the following equation representing the total rate of change of $[K^+]_o$ due to ionic exchanges processes in a single neuron:

$$\begin{aligned} \frac{d[K^+]_o}{dt} &= \frac{50}{96489} \frac{\text{mol}}{\text{cm.mC}} \times \left(I_{\text{KCa}} + I_K + I_{\text{Km}} - I_{\text{Kpump}} + I_{L\,|\,K}\right) \\ &\quad + \frac{\partial [K^+]_o}{\partial t}\Big|_{\text{glia}}. \end{aligned} \tag{20}$$

In the above Equation 20, 50/96,489 is the conversion factor from electric current to rate of change of interstitial potassium ionic concentrations. In particular, the numerator 50 can be interpreted as the entire somatic surface of a neuron being enclosed by an interstitial space that has a depth of $d_{\text{FHS}} = 0.2$ μm.

Cortical network model

In this study, the cortical network model occupies a 3-dimensional volume of 500 μm × 500 μm × 850 μm (depth). The network model has a simplified cortical layer structure along its depth and corresponds roughly to a small cortical microcolumn. The top layer corresponds to cortical layers 2–3 and consists of spatially randomly distributed pyramidal neurons (P1) and FS inhibitory interneurons (I1), while the bottom layer corresponds to layers 5–6 and consists of pyramidal neurons (P3), also randomly distributed spatially. There are altogether 303 neurons in the network, of which 65 are P1 (indexed from 0 to 64), 32 are I1 (indexed from 65 to 96) and 206 are P3 (indexed from 97 to 302). The soma of every neuron in the top layer is located between 102 and 323 μm along the depth profile of the cortical volume. Somas of neurons in the bottom layer are located at depths larger than 323 μm. Parameters of synaptic coupling strength and background input activity are adjusted to account for the low density of neurons in the cortical microcolumn and its embedding in the much larger neural system (Bazhenov et al., 2004; Fröhlich et al., 2010; Ho and Truccolo, 2016).

We note that in this study, for computational efficiency, we have placed all the FS inhibitory interneurons in the superficial layer, as was also the case in Anderson et al. (2007). Nevertheless, the extensive connectivity between these FS inhibitory interneurons and pyramidal neurons of superficial and deep layers (Table 3) should mitigate the absence of FS inhibitory interneurons in the deeper layer of our cortical network model.

Synaptic connections. Equation 1 represents a single neuron without any synaptic connection. Having indexed every neuron in the network ($V \to V^l$ where l represents neuron index), an extra current $I^l_{syn}(t)$ was added to the RHS of the equation to represent synaptic input contributions to ionic currents:

$$I^l_{\text{syn}} = \sum_{m \neq l} \Gamma_{m \to l} \times g^{m \to l}_{\text{syn}} \times s_m(t - \tau^{m \to l}_{\text{delay}}) \times (E^m_{\{e,i\}} - V^l). \tag{21}$$

The above Equation 21 represents the total synaptic currents on neuron l resulting from other individual neurons, indexed by m, in the network; $s_m(t)$ represents the synaptic gating variable of neuron m, $g^{m \to l}_{\text{syn}}$ the synaptic conductance strength between pre-synaptic neuron m and post-synaptic neuron l, $E^m_{\{e,i\}}$ the excitatory or inhibitory reversal potential (whether it is excitatory or inhibitory depends on the type of pre-synaptic neuron m, thus the superscript), $\tau^{m \to l}_{\text{delay}}$ the axonal conduction delay between neurons m and l, and $\Gamma^{m \to l}$ the matrix element indicating the presence (1) or absence (0) of connections between m and l. Parameters related to synaptic dynamics and interactions are specified in Table 2. Synaptic connectivity between different types of neurons in the network was randomly set according to connection probabilities specified in Table 3).

Table 2. Synaptic and other related parameters used in simulations of neuronal network models, unless otherwise specified

Parameter	Description	Units	Value
E_i	Inhibitory reversal potential	mV	−73
E_e	Excitatory reversal potential	mV	0
τ_{e1}	Excitatory synaptic rise time constant (Eq. 22)	ms	0.02
τ_{e2}	Excitatory synaptic decay time constant (Eq. 22)	ms	3
τ_{i1}	Inhibitory synaptic rise time constant (Eq. 22)	ms	0.02
τ_{i2}	Inhibitory synaptic decay time constant (Eq. 22)	ms	6
τ_e	Graded excitatory synaptic decay time constant (Eq. 24)	ms	2.4
τ_i	Graded inhibitory synaptic decay time constant (Eq. 24)	ms	5.5
τ_{delay}	Axonal conduction delay (Eq. 21)	ms	0
$s_{\max}$	Maximal value of gating variable per spike	-	1
g_{e0}	Mean background excitatory drive to model pyramidal neurons/interneurons (Eq. 26)	mS/cm^2	0.0071/0.0087
r_e	Mean excitatory background activity firing rate (Eq. 26)	s^{-1}	300
g_{i0}	Mean background inhibitory drive to model pyramidal neurons/interneurons (Eq. 26)	mS/cm^2	0.017/0.017
r_i	Mean inhibitory background activity firing rate (Eq. 26)	s^{-1}	300
$g_{\text{syn}}^{i\rightarrow i}$	Unitary conductance from an inhibitory interneuron to another interneuron	mS/cm^2	4.3×10^{-3}
$g_{\text{syn}}^{e\rightarrow e}$	Unitary conductance from a pyramidal cell to another pyramidal cell	mS/cm^2	variable
$g_{\text{syn}}^{e\rightarrow i}$	Unitary conductance from a pyramidal cell to another interneuron	mS/cm^2	2.2×10^{-3}
$g_{\text{syn}}^{i\rightarrow e}$	Unitary conductance from an interneuron to another pyramidal cell	mS/cm^2	variable
$\Gamma_{m\rightarrow n}$	Connectivity matrix element (with values of either 1 or 0) between neuron m and n	–	assigned according to the probability values in Table 3
D	Diffusion constant of K^+ in extracellular space (Eq. 25)	cm^2/ms	2.5×10^{-9}

A "variable" label on the value column denotes that the parameter is dependent on a specific simulation. Please refer to the main text for specific values.

Table 3. Pairwise connection probability matrix between different neuronal populations in the simulated network models

Γ	P1	I1	P3
P1	0.15	0.15	0.15
I1	**0.35**	0.4	0.35
P3	0.15	0.15	0.15

Each matrix element represents the connection probability between two types of neurons in the network. The arrow's direction indicates the direction of the interaction. For example P(I1→ P1)=0.35 (bold font) indicates that there is a 0.35 probability that there is an inhibitory connection between an I1 type neuron and a P1 type neuron.

We used two forms of synaptic temporal profile for network simulations. In the first, simpler form, $s_{\cdot}(t)$ follows a two-state kinetic scheme which can be mathematically described as:

$$s_m(t) = s_{\max} \times \sum_j \int_{-\infty}^{t} \underbrace{\left(\exp\left(-\frac{t-t'}{\tau^m_{\{e,i\}2}}\right) - \exp\left(-\frac{t-t'}{\tau^m_{\{e,i\}1}}\right)\right) \times H(t-t')}_{K^{syn}_{\{e,i\}}(t-t')} \times \delta(t' - t^{m,j}_{AP})\, dt', \quad (22)$$

where H is the Heaviside step function, $t^{m,j}_{AP}$ is the jth action potential time since $t = -\infty$ when the membrane potential V^m crosses the action potential threshold from below, and the $\tau_{\{e,i\}2,1}$ are the synaptic rise (subscript 1) and decay (subscript 2) time constants, respectively. (Again, whether the time constants are excitatory or inhibitory depends on the types of the pre-synaptic neuron m, thus the superscript.)

Equation 22 can be interpreted as a convolution between the spike train history of neuron m with the (time-causal) kernel $K^{\text{syn}}_{\{e,i\}}$ specifying the rise and decay profile of the synaptic dynamics. In the above Equation 22, since $K^{\text{syn}}_{\{e,i\}}$ is convolved with only the spike train history, $s_{\cdot}(t)$ is only dependent on spike timing, but not directly on the shapes of individual action potentials of pre-synaptic neuron m.

In actual neural systems, however, changes in the shapes and magnitudes of pre-synaptic action potentials can lead to changes in the influx of pre-synaptic Ca^{2+}, which in turn alter the likelihood of presynaptic vesicles release (and their quantity) into the synaptic cleft (Yang and Wang, 2006; Chao and Yang, 2019; Scarnati et al., 2020; Mochida, 2022). One consequence of this series of biophysical events is the transient alteration of the effective synaptic coupling between neurons. To represent the effects of these events on network dynamics, we also used synaptic variables that capture the overall influence of the shapes and amplitudes of presynaptic action potentials on the final effective synaptic coupling between neurons in network simulations.

In this second form of synaptic temporal profile, $s_{\cdot}(t)$ is "graded" in the sense that the shapes of action potentials of the pre-synpatic neuron are also incorporated into $s_{\cdot}(t)$ via the following equation (Destexhe et al., 1994; Golomb et al., 1994; Sharp et al., 1996; Abbott and Marder, 1998):

$$\frac{ds_m(t)}{dt} = \frac{1}{\tau_{\{e,i\}}} \times \frac{s_\infty(V^m(t)) - s_m(t)}{s_{\max} - s_\infty(V^m(t))}, \quad (23)$$

with

$$s_\infty(V^m) = s_{\max} \times \tanh \frac{|V^m + 35\,\text{mV}| + V^m + 35\,\text{mV}}{20\,\text{mV}}. \quad (24)$$

In the above Equation 24, $s_\infty(V^m) = 0$ when $V^m \leq -35$ mV, and $s_\infty(V^m) \rightarrow s_{\max}$ when $V^m \rightarrow +\infty$. Hence, our choices of parameters ensure that only the shapes of action potential events, and not subthreshold dynamics, of neuron m are incorporated in the temporal profile $s_m(t)$.

We note that only neuronal somas are represented in our cortical model of single compartment neurons. Thus, when interpreting V values of our cortical model in the context of spatially extended neurons, the assumption that V^m being homogeneous across soma and axons is taken. In other words, when extending our interpretation of V to spatially extended neurons, we assume that modulation of g_K is homogeneous across soma and axonal membranes, for both myelinated and non-myelinated axons. We think this assumption is a reasonable first-order approximation given that, for example, 4-AP effects on potassium conductances appear to extend in a similar way to both soma and axons.

Potassium diffusion. In addition to the potassium pump and glial uptake mechanism that are already in place to regulate interstitial potassium concentrations for each neuron at the single cell level, there is also a diffusion mechanism in the network model that allows interstitial potassium ions to diffuse across the local network via the extracellular space. Movement of potassium ions between the interstitial and extracellular spaces is facilitated by a flux current which obeys the Fick's law. Thus, the following term is added to the RHS of Equation 20:

$$\frac{\partial [K^+]_o}{\partial t}\Big|_{\text{diff}} = \frac{D}{2\pi \times R_{\text{soma}} \times (L_{\text{soma}} + R_{\text{soma}}) \times d_{\text{FHS}}} \times \oiint \nabla [K^+] \cdot d\hat{n}, \quad (25)$$

where D is the diffusion constant of potassium, $\nabla[K^+]$ denotes the potassium concentration gradient between the interstitial and extracellular spaces, and $d\hat{n}$ is the dimensionless unit vector normal to the differential element of the interstitial-extracellular interface. The orientation of $d\hat{n}$ is always towards the extracellular space (Fig. 1*B*). Equation 25 can be transformed into the more familiar form of the diffusion equation by means of the divergence theorem.

We emphasize that, since our study focuses on the changes in local network dynamics induced by g_K downmodulation, the contribution of potassium diffusion (via larger extracellular spaces) to seizure propagation across brain areas remains an important open question.

Background synaptic activity. Each neuron in the cortical network model is driven by an external input which mimics the background synaptic activity. In this work, the background synaptic activity for each neuron is represented by two independent point processes (spike trains) related to excitatory and inhibitory background presynaptic inputs, respectively, according to:

$$\begin{aligned} I^l_{\text{ext}}(t) &= g^l_e(t) \times (E_e - V^l) + g^l_i(t) \times (E_i - V^l), \\ g^l_{\{e,i\}}(t) &= g_{\{e,i\}0} \times s_{\max} \times \sum_j \int_{-\infty}^{t} K^{\text{syn}}_{\{e,i\}}(t - t') \times \delta(t' - t^{\{e,i\},[l],j}_{\text{AP}})\, dt', \end{aligned} \tag{26}$$

where $t^{\{e,i\},[l],j}_{\text{AP}}$ represents the jth spike time of the external spike train that drives the background excitatory (inhibitory) activity of neuron l. Here, we assume this background activity to be generated by homogeneous Poisson spike train inputs, with corresponding mean rates $r_{\{e,i\}}$ also homogeneous across each neuron type (Table 2).

Single neuron and cortical network implementations. We used the NetPyNE software package for network simulations (version 1.0, Dura-Bernal et al., 2019). NetPyNE is a Python-based tool for modeling brain neuronal circuits that uses NEURON (version 8.0a nightly package, Carnevale and Hines, 2006; Hines and Carnevale, 2014) as the backend for numerical integration of biophysical neuron models. The NetPyNE platform contains advanced APIs that communicate with the rich repertoire of modules in NEURON. Hence, it serves as a very user-friendly and efficient interface for accessing the powerful features of the NEURON platform at both the single neuron and network levels. In addition to simulations, NetPyNE is capable of performing visualization and analytics of simulation results.

In our cortical network model, configurations of individual neurons were carried out using the .mod framework in the NEURON environment. We used the `USEION` directive for potassium ions, such that the value of E_K for each neuron is automatically calculated. The movements of ions between spaces are implemented by the reaction-diffusion (RxD) module of NEURON (McDougal et al., 2013; Newton et al., 2018; Kelley et al., 2022) once the geometries of the intracellular and interstitial spaces are provided. (Each of these RxD configurations can be accessed via the NetPyNE interface.) Specifically, the accounting of the potassium ions between the intracellular and interstitial spaces was handled automatically within NEURON. One difference between NEURON based accounting of potassium ionic concentrations and the manual accounting based on Equation 20 is that NEURON also considers the minute changes in $[K^+]_i$ while Equation 20 assumes that $[K^+]_i$ is a constant. The difference has no material effect on the simulation results, since the intracellular volume is vastly larger than the interstitial space. A very small change in $[K^+]_i$ incurs a large change in $[K^+]_o$.

While the built-in methods of the RxD module conveniently process the transport of potassium ions between intracellular and interstitial spaces, an extra complexity arises when we also allow the ions to move across the interstitial-extracellular interface (i.e., $\frac{\partial[K^+]_o}{\partial t}|_{\text{diff}}$ of Eq. 25) to facilitate diffusion across the network. We accomplished this by means of setting up a one-to-one, reversible conversion reaction (using `rxd.MultiCompartmentReaction`) between interstitial potassium ions and a type of surrogate particles that only resided in the extracellular region. The surrogate particles then represented extracellular potassium ions. The value of reversible reaction rate was so determined as to approximate the result of $D \times \nabla$ operator on $[K^+]$ of Equation 25. (See also below for more details.)

The complex topology of the extracellular space means that only a small portion of the entire extracellular volume is accessible for potassium ions. In the RxD module, the fraction is captured by the parameter α_{vol}. The no-flux or Neumann boundary condition was imposed on the boundaries of the cortical network. The effect of this boundary condition is that there is no diffusion of potassium ions across the network boundaries, ensuring zero net gain or loss of the ions in the network due to diffusion.

To facilitate the numerical simulation of the diffusion equation, the 3-D cortical network was divided into cubic voxels of length dimension d_{voxel}. Each voxel is a homogenized unit for the purpose of potassium ion diffusion in the extracellular space. The graininess of voxel discretization has a direct effect on the accuracy of the simulation results. For example, since d_{voxel} represents the spatial resolution limit of the RxD module, in approximating the covariant $\nabla[K^+]$ of Equation 25, the magnitude of the inverse length of each dimension was taken to be uniform $\frac{2}{d_{\text{voxel}}}$ for every neuron in order to average out the different locations of neurons within a voxel. Therefore, an appropriate length dimension of each voxel should be approximately the average diameter of the soma of a neuron, so that each voxel is sufficiently voluminous to contain a few somas.

Network simulations were carried out for five main different scenarios. These scenarios included normal g_K, and g_K downmodulation in either the pyramidal or the inhibitory interneuronal population in the network (Figs. 6, 7, 9). Each simulation had a simulated time of 2,500 s. These simulations within a scenario shared identical parameters and initial conditions except for different setups in the $g^{e\to e}_{\text{syn}}$ and $g^{i\to e}_{\text{syn}}$ values. The purpose of varying $g^{e\to e}_{\text{syn}}$ and $g^{i\to e}_{\text{syn}}$ in these different simulations was to facilitate comparison of the emergence of epileptic seizure-like dynamics in the five different examined scenarios.

Single neuron simulations (Figs. 2, 3, 4, 5, 8*C–E*) were performed using `xppaut` (version 8.0, Ermentrout, 2002). Visualisation of single neuron and network simulations results was performed using `xfig` (version 3.2.8b, https://mcj.sourceforge.net/), `gnuplot` (version 5.4, Williams and Kelley, 2020) and R software (version 4.1.0, R Core Team, 2022) with `dplyr` (Wickham et al., 2022), `vroom` (Hester et al., 2022), `ggplot2` (Wickham, 2016) and `oce` (Kelley and Richards, 2024) packages. Statistical analyses were performed with R software.

Post-simulation analyses

Synchrony measure. We used a synchrony measure (Golomb and Rinzel, 1993, 1994; Rich et al., 2020a,b) to quantify the degree of spiking coherence in the pyramidal neuron population of the simulated networks. The synchrony measure S is defined as follows:

$$S \equiv \frac{\langle \overline{\mathcal{V}_l(t)}^2 \rangle - \langle \overline{\mathcal{V}_l(t)} \rangle^2}{\overline{\langle \mathcal{V}_l(t)^2 \rangle - \langle \mathcal{V}_l(t) \rangle^2}}, \tag{27}$$

where $\mathcal{V}_l$ is the "smoothed out" spike train history of pyramidal neuron l:

$$\mathcal{V}_l(t) = \sum_j \int K^{\text{spike}}(t - t') \times \delta(t' - t^{l,j}_{\text{AP}})\, dt'. \tag{28}$$

In Equation 27, $\langle\cdot\rangle$ denotes time averaging and a bar on top denotes averaging across the pyramidal population. The value of S ranges between 0 and 1.

In this work, both the kernel $K^{\text{spike}}(t)$ and the spike train of pyramidal neuron l were first discretized to the nearest millisecond to facilitate efficient calculation of S. The kernel was then transformed into a Toeplitz matrix. The purpose of doing so was to exploit the structure of the Toeplitz matrix to convert the integration sign of Equation 28 into the numerically efficient matrix multiplication between the transformed kernel and the discretized spike train. To avoid transient effects, only the last 1,250 s of the spike train history of the pyramidal population was used in the convolution operation of Equation 28, which means that the j in $\sum_j$ only included spikes occurring during the final 2,000 seconds of simulation. The discretized $K^{spike}(t)$ spanned a temporal window of 10 ms, and can be represented in a row vector form as (1,10, 10, 10,10, 10, 10, 10, 10, 1). All work in this section was performed using R software (version 4.1.0, R Core Team, 2022) with the `Matrix` (Bates and Maechler, 2021) and `reticulate` (Ushey et al., 2021) packages.

The upper panel of Figure 6*A* shows the calculated synchrony measure S of each simulation across different $g_{\text{syn}}^{e\to e}$ and $g_{\text{syn}}^{i\to e}$ parameters in the reference set of network simulations. The upper panels of Figure 6*B–F* show examples of spiking patterns of simulations in the set. By comparing the synchrony measure value for each simulation with the corresponding spiking pattern, it is clear that there is a strong positive relationship between S and the appearance of seizure-like firing patterns in the pyramidal neuron population–a higher value of S corresponds to the emergence of seizure-like firing patterns in the pyramidal population.

Injected current-pulse perturbation analysis. We developed a current pulse perturbation analysis (akin to phase resetting curves, see for example Chapter 10 of Izhikevich, 2007) to assess the sensitivity of single-neuron spiking to noise perturbations during the almost periodic regimes characteristic of simulated epileptic seizure-like dynamics (Fig. 8*C–E*). In this analysis, a measure was formulated to quantify the degree of advance or delay of the timing of the succeeding spike upon a very short (3 ms) current pulse injection. The advance or delay is defined with respect to action potential times of a model neuron in the periodic regime. (Periodic spiking activity regime is achieved with a properly chosen *constant* current injection.) At each time point n for current pulse injection during the inter-spike interval, the measure is defined as follows:

$$A(n) \equiv \frac{t(s)_0 - t(s)}{t(s)_0 - t(n)}, \tag{29}$$

where $t(s)$ is the time of the succeeding spike upon current pulse injection, $t(s)_0$ is the time of the succeeding spike if the neuron were unperturbed (zero pulse injection) and $t(n)$ is the time of the current pulse injection point.

Therefore, the advance or delay of the succeeding action potential is normalized against the spiking behaviour of the unperturbed neuron. Accordingly, $A(n) = 1$ if current pulse injection results in the immediate onset of an action potential (i.e., $t(s) = t(n)$), and $A(n) = 0$ if current pulse injection fails to alter the timing of the next action potential onset (i.e., $t(s) = t(s)_0$). Moreover, $A(n)$ is negative (i.e., $t(s) > t(s)_0$) in the case when the onset of action potential is delayed by current pulse perturbation.

$\overline{[K^+]_o}$. In the Results section, we report average values of interstitial potassium concentration $\overline{[K^+]_o}$, which was computed as follows. The lower panel Figure 6*A* shows the time-averaged values of the mean interstitial potassium concentration across all the pyramidal neuron sites for each network simulation of the set. Similar to the synchrony measure S, the temporal averaging $\langle \cdot \rangle$ included only the final 1,250 s of each simulation. Each lower panel of Figure 6*B–F* shows the temporal progression of mean $[K^+]_o$ values across all inhibitory interneuron sites (blue line) and pyramidal neuron sites (red line), for the specific network simulation as represented by the panel. The work in this section was performed using Python software (version 3.7.4, Python Software Foundation, https://www.python.org) with `pandas` (McKinney, 2010) package.

Results

In the following sections, we examine the effects of g_K downmodulation separately for individual excitatory and inhibitory single-neuron models, and for a cortical network model made of coupled neurons spatially distributed in layers within a 3-dimensional cortical volume. Besides the intrinsic dynamics, single neuron models included movement of potassium ions across an interstitial space (Fig. 1*A*). Network models additionally included synaptic coupling dynamics and potassium diffusion across extracellular spaces (Fig. 1*B*). Details and parameter specifications are given in the Materials and Methods section and Tables 1–3, respectively.

Single cell simulations on the effects of g_K downmodulation on pyramidal neurons and fast-spiking inhibitory interneurons

We first examined a pyramidal neuron model with normal and reduced g_K parameter values. Figure 2*A*,*B* show example simulations of normal and reduced g_K, respectively. g_K downmodulation resulted in lower firing rates under different constant current injections (Fig. 2*C*), and slightly higher potassium concentrations in interstitial and extracellular spaces. Importantly, it also resulted in a very noticeable broadening of action potentials (time taken between −35 mV of the depolarization phase and −35 mV of the repolarization phase: 0.595 ± 0.005 ms (SEM), $n = 3$ in normal g_K case vs 5.095± 0.005 ms (SEM), $n = 3$ in $g_K = 0.3\ \text{mS/cm}^2$ case; Fig. 3*A*). As stated earlier, similar broadening of action potentials with g_K downmodulation has also been observed in previous experimental studies examining the effects of 4-AP on nerve fibers in the spinal cord and hippocampal pyramidal neurons (Bostock et al., 1981; Mitterdorfer and Bean, 2002). In our model this broadening effect on action potentials can be explained as follows: first, as g_K is reduced, there is also a reduction in the voltage-gated potassium current (I_K; Fig. 3*C*), which is responsible for the fast re-polarization phase of action potentials. Second, the prolonged depolarization of the pyramidal neuron also leads to an increased accumulation of intracellular calcium Ca_i^{2+} (Fig. 3*D*), resulting in prolonged activation of I_{KCa} (Fig. 3*B*). The much stronger, but slower acting I_{KCa} becomes more dominant than the fast I_K for the repolarization of the pyramidal neuron model, further slowing down the repolarization phase (Fig. 3*E*), thus contributing to the broadening of action potentials. In addition to the overall broadening, the re-polarization can briefly slow down around −40 mV as shown in the example for $g_K = 0.3\ \text{mS/cm}^2$ (Fig. 3*A*,*E*).

Furthermore, under reduced g_K, this increased I_{KCa} also elicits a stronger afterhyperpolarization as compared to the normal g_K scenario in which the faster and less sustained I_K was dominant (Fig. 3*A*,*E*), thus providing a more robust regulation against depolarization for a large portion of each interspike interval, and as a consequence reducing the firing rates of the pyramidal neuron model under constant current injection as seen above in Figure 2*C*. Next, we examined the effect of g_K downmodulation on a single FS inhibitory interneuron. Figure 4*A*,*B* summarize the results for normal and reduced g_K levels, respectively. In contrast to the pyramidal neuron model, a moderate reduction of the potassium conductance to $g_K = 7.5\ \text{mS/cm}^2$ increased firing rates. Although with a much smaller effect as for the pyramidal neuron model, moderate g_K downmodulation also led to a broadening of action potentials during spiking activity (Fig. 5*A*). However, a further reduction in g_K resulted in a collapse of firing rates that subsequently led to the emergence of depolarization block in the FS interneuron. In the case of the FS interneuron parameters (Table 1) used here, a reduction of g_K to $\sim 4\ \text{mS/cm}^2$ was already sufficient to induce depolarization block for any injected current above the rheobase value. (not shown)

The increased firing rate under moderate g_K reduction can be explained by the zero g_{KCa} in this FS inhibitory interneuron model (Fig. 5*B*,*D*) as compared to the pyramidal neuron model. As a result, g_K downmodulation does not induce any I_{KCa} in the inhibitory interneuron model. The combined effects of I_K

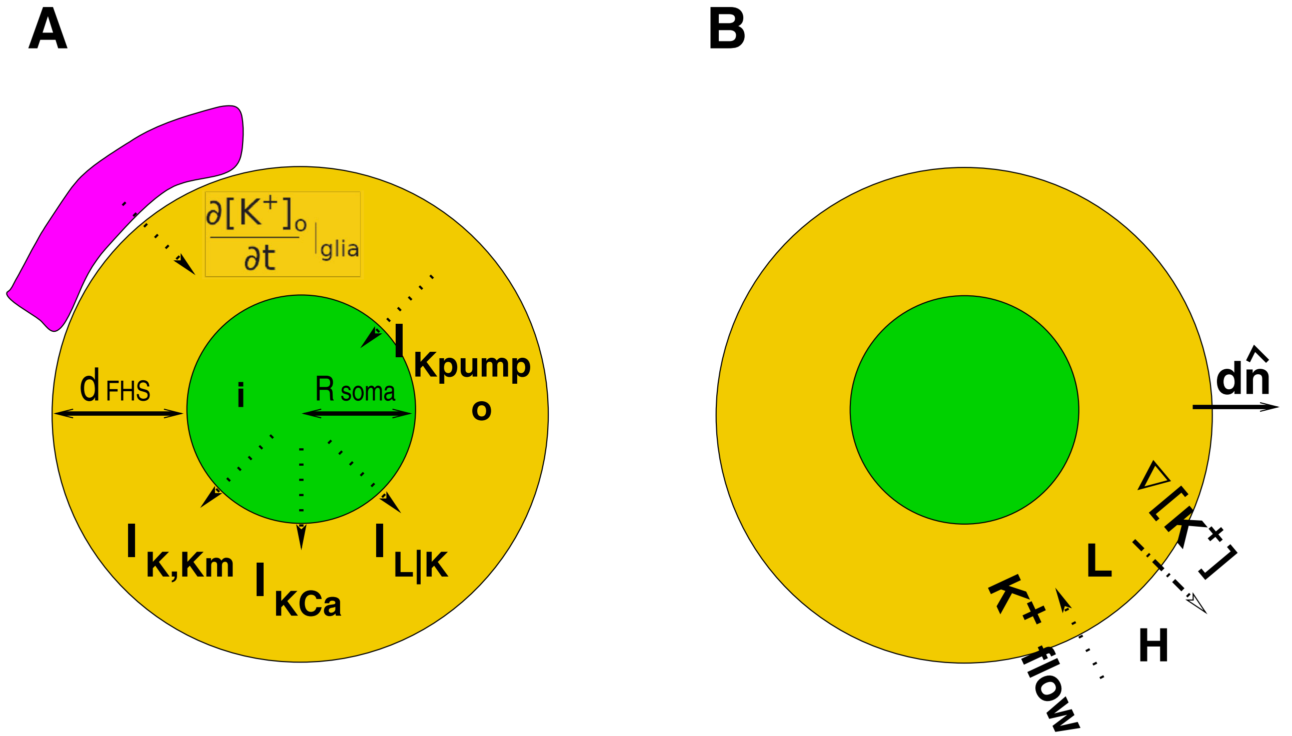

Figure 1. Sources of potassium currents and potassium diffusion in the single neuron and network models. ***A***, Cross-sectional view of the somatic area of a single neuron and its surroundings: the soma (green, labelled "i"), the interstitial or Frankenhaeuser-Hodgkin space (gold, labelled "o"), and the nearby glial cells (magenta). The dashed arrows represent sources of changes in interstitial potassium concentration $[K^+]_o$, with the head of each arrow denoting the direction of potassium flow when the value of the represented source is positive. The terms d_{FHS} and R_{soma} denote the depth of the interstitial space and the radius of the soma, respectively (Table 1). The length dimension L_{soma} of the cylindrical shaped soma is not shown in this figure. Depictions of soma and interstitial spaces are not to scale. ***B***, Movement of potassium across the interstitial-extracellular interface in network models. $d\hat{n}$ is the normal unit vector to the differential surface element of the interface. The direction of $d\hat{n}$ always points to the extracellular space (white background). In this particular scenario depicted when $[K^+]_o$ is lower (i.e., ***L***) than the extracellular potassium concentration which is higher (i.e., ***H***), $\nabla[K^+]$ also points outward to the extracellular space. Therefore $\frac{\partial[K^+]_o}{\partial t}|_{diff}$ is positive according to Equation 25, meaning a net flow of potassium ions from the extracellular to the interstitial space.

reduction (Fig. 5*C*) with the absence of compensatory increase of I_{KCa} shorten the afterhyperpolarization phase following action potentials. In this case, the interneuron can more easily depolarize and spike again, resulting in the observed increased firing rate under moderate g_K reduction.

The higher sensitivity of the FS inhibitory interneuron to depolarization block under g_K reduction can be understood as follows. Depolarization/excitation block can be effectively viewed as an "infinite" widening of action potentials, meaning the complete removal of the repolarization phase in the neuron. In the pyramidal neuron model, the g_{KCa} conductance is an important contributor to repolarization and afterhyperpolarization processes by driving the membrane voltage closer to E_K. Since g_{KCa} is set to zero in the inhibitory neuron model, that implies already a weaker or slower repolarization as compared to the pyramidal neuron. Downmodulation of g_K further weakens the repolarization process, thus the higher sensitivity of the inhibitory neuron model to depolarization block under reduced g_K.

We also emphasize the rheobase shift of both the g_K downmodulated pyramidal neuron and inhibitory interneuron relative to their normal g_K counterparts (Figs. 2*C*, 4*C*). g_K downmodulation lowers the rheobase of the neuron because a decrease in I_K does not lead to any compensatory increase in I_{KCa} when the external applied current is below the rheobase. In this regime, the neuron's firing rate is zero and therefore intracellular Ca^{2+} cannot accumulate and lead to activation of I_{KCa}. This lowered rheobase reflects the amount of reduction in I_K, and is indicative of the neuron's higher basal excitability as a consequence of reduced g_K.

In summary, both similar and different effects of g_K downmodulation were observed in the pyramidal neuron and FS inhibitory interneuron models. Although the broadening of action potentials can be observed in both cases, a more pronounced effect can be achieved in the pyramidal neuron since lower g_K levels can be implemented in this case. In addition, while in the pyramidal neuron a gradual g_K downmodulation led to a gradual decrease in firing rates under most values of constant injected currents examined, a very different behavior was observed for the inhibitory interneuron. For a moderately decreased $g_K = 7.5$ mS/cm^2, increase in firing rates was obtained, but further decrease in g_K, e.g., $g_K \sim 4$ mS/cm^2, eventually led to the collapse of firing rates and complete depolarization block.

A reference cortical network dynamics based on normal g_K, but with gradually emerging seizure-like dynamics due to increasing excitatory coupling

We developed a cortical network model consisting of two layers, approximately corresponding to layers 2–3 and 5–6 in neocortex, spanning in total a volume of 500 µm × 500 µm × 850 µm (depth). The layers included 303 cells, of which 32 were FS inhibitory interneurons. Neurons were uniformly randomly distributed in the 3-dimensional space while respecting the two layer organization (Materials and Methods). Table 3 shows the relevant synaptic and connection parameters used in the

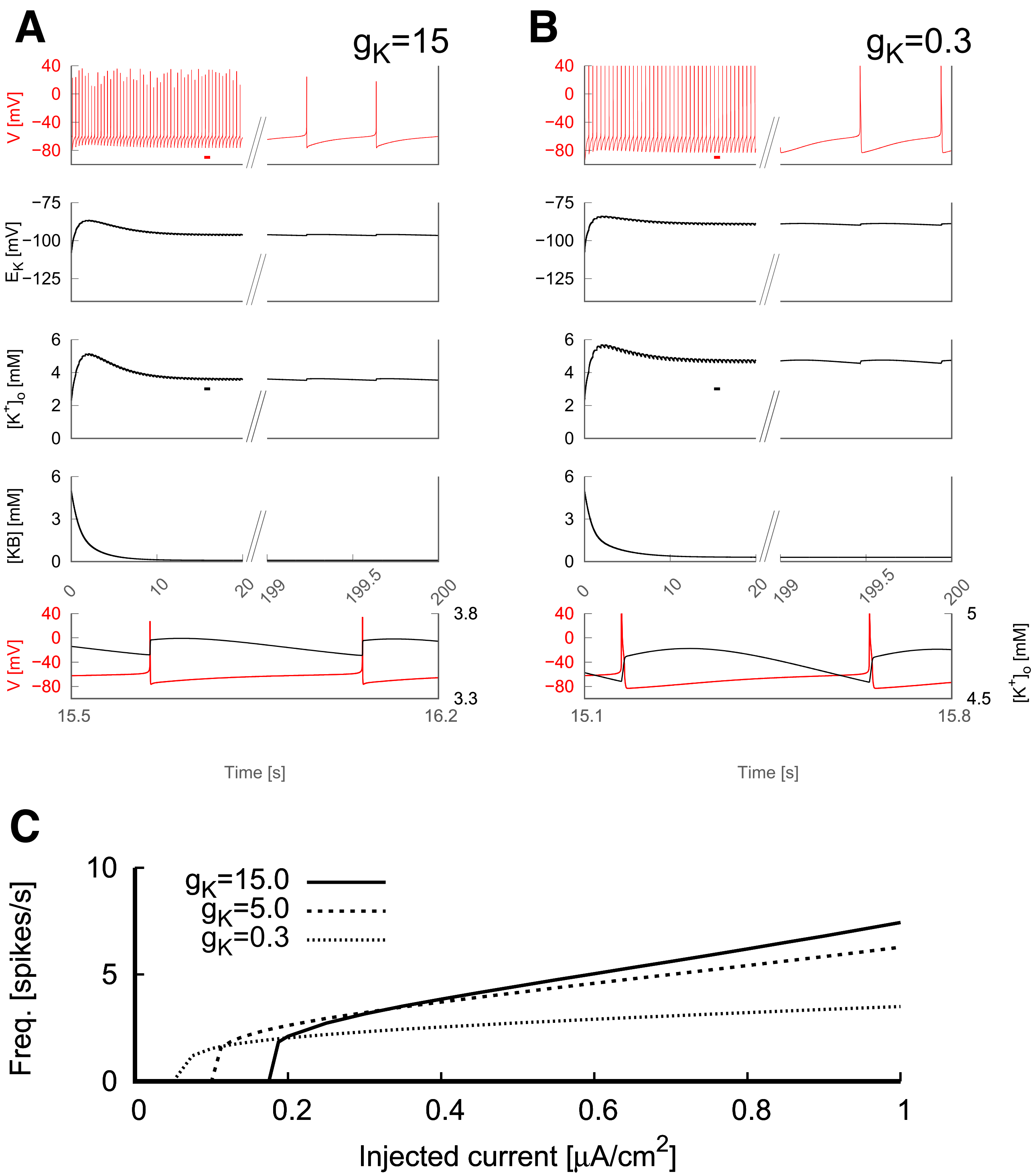

Figure 2. Single neuron dynamics: effects of g_K downmodulation on the spiking activity of single pyramidal neuron models. ***A***, A 200-second simulation of a pyramidal cell model with a "normal" g_K value of 15.0 mS/cm^2 and I_{ext} value of 0.225 μA/cm^2. Top and middle panels showing the membrane potential, potassium reversal potential E_K, interstitial potassium concentration $[K^+]_o$ and glial [KB] readings. Bottom panel: Magnification of a 0.7-s segment (denoted by red and black short horizontal bars in the top and middle panels, respectively) of the simulation, showing only the membrane potential and $[K^+]_o$ values. ***B***, Same as ***A***, but with $g_K = 0.3$ mS/cm^2. ***C***, Frequency-current (F-I) curves for pyramidal cell models with g_K = 15.0, 5.0 and 0.3 mS/cm^2. Although firing rates decrease with decreasing g_K, the neuron does not go into depolarization block for the examined range of injected constant currents.

network simulations. In addition to the interstitial space, the extracellular space between individual neurons in the network models allow diffusion of potassium ions across the entire network (Fig. 1*B*).

We start by considering a reference case network model which will be used for comparison in the following sections. We ran independent stochastic network simulations across a range of $g_{syn}^{e\to e}$ and $g_{syn}^{i\to e}$ values, with fixed normal levels of $g_K = 15\,\mathrm{mS/cm^2}$ and $10\,\mathrm{mS/cm^2}$ for pyramidal neurons and FS inhibitory interneurons, respectively. Of these simulations, five with illustrative values for $g_{syn}^{e\to e}$ and $g_{syn}^{i\to e}$ are shown in Figure 6*B–F*, respectively.

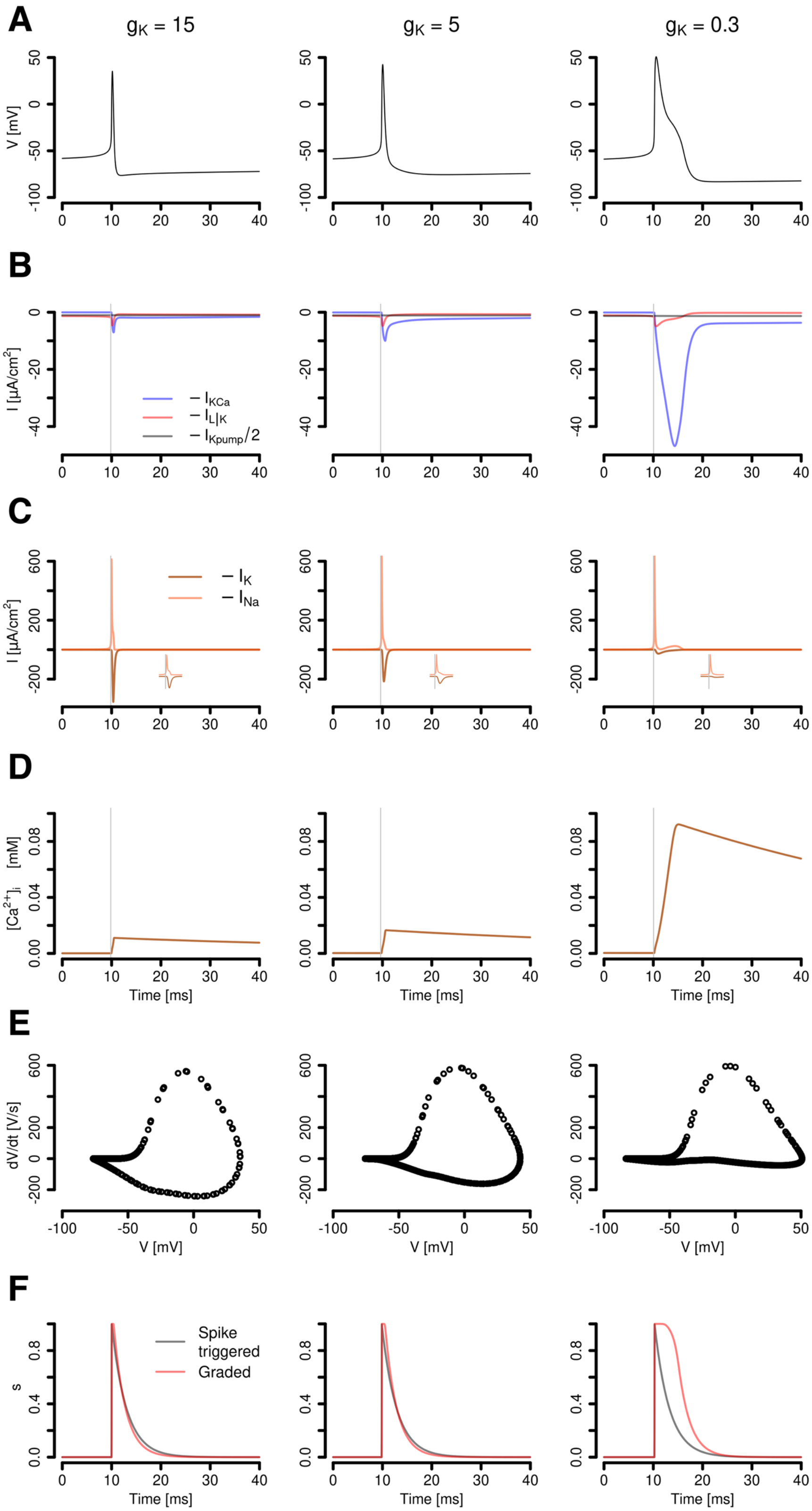

Figure 3. Effects of g_K downmodulation on ionic currents, intracellular calcium concentration $[Ca^{2+}]_i$, and synaptic properties during action potentials in the single pyramidal neuron model. A clear broadening effect on action potentials and related changes in ionic currents and concentrations are observed. ***A***, Temporal profile of action potentials. ***B***, Time course of potassium-related currents during the action potentials shown in ***A***. Inward currents are denoted by positive magnitudes. Here and below, the light grey vertical line denotes the time point at which $[Ca^{2+}]_i$ starts to increase. ***C***, Time course of voltage gated currents I_K and I_{Na}. Inward currents are denoted by positive magnitudes. Inset is the magnification of I_K and I_{Na} around the time when $[Ca^{2+}]_i$ starts to increase, showing that membrane depolarization by I_{Na} precedes the rise of $[Ca^{2+}]_i$. The I_K and I_{Na} traces were separated by a vertical offset in the inset for better visualization. ***D***, $[Ca^{2+}]_i$ during the action potentials shown in ***A***. ***E*** Phase portrait: membrane potential vs its time derivative during a time interval including several consecutive action potentials. Each portrait is based on down-sampled data of resolution 0.03 ms. Numerical time derivative values are an average of the first order approximation of the left and right derivatives at each sampled time point. ***F***, Temporal profiles of synaptic variables associated with the action potentials shown in ***A***. Graded synaptic variables are given by Equation 24, while the spike-triggered ones follow the synaptic gating mechanism given by Equation 22.

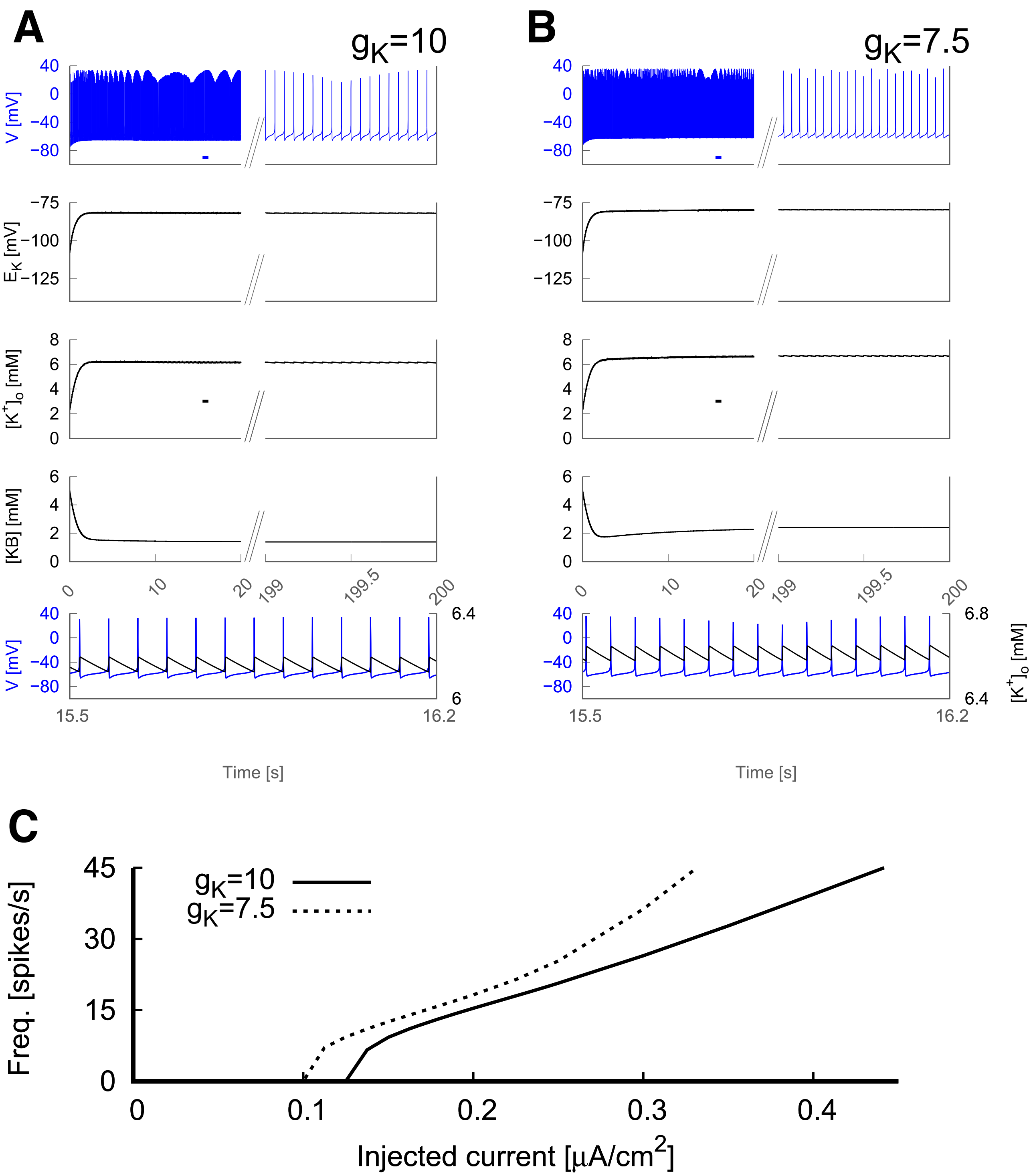

Figure 4. Single neuron dynamics: effects of g_K downmodulation on the spiking activity of FS inhibitory interneuron models. ***A***, A 200-second simulation of an interneuron model with a "normal" g_K value of 10.0 mS/cm^2 and I_{ext} value of 0.225 µA/cm^2. Top and middle panels showing the membrane potential, potassium reversal potential E_K, interstitial potassium concentration $[K^+]_o$ and [KB] readings. Bottom panel: Magnification of a 0.7-second segment (denoted by blue and black short horizontal bars in the top and middle panels, respectively) of the simulation, showing only the membrane potential and $[K^+]_o$ values. ***B*** Same as ***A***, but with $g_K = 7.5$ mS/cm^2. ***C***, Frequency-current (F-I) curves for FS inhibitory interneuron models with $g_K = 10.0$ and 7.5 mS/cm^2. In the case of reduced g_K, firing rates not only increased for every injected constant current value examined here, but also accelerated with respect to higher magnitudes of injected current.

We examined how synaptic coupling strength affects synchronization in this reference network. We used a statistical measure of synchrony S (Materials and Methods). As seen in Figure 6*A*, for fixed $g_{\text{syn}}^{i\to e}$, S increased with increasing $g_{\text{syn}}^{e\to e}$. Furthermore, although this base network has normal g_K levels, it can still show epileptic seizure-like dynamics under sufficiently strong excitatory-excitatory synaptic couplings (Fig. 6*D–F*). Seizure-like dynamics were characterized by recurrent almost-periodic synchronized neuronal-population spiking in the cortical network (~3 spikes per second), with

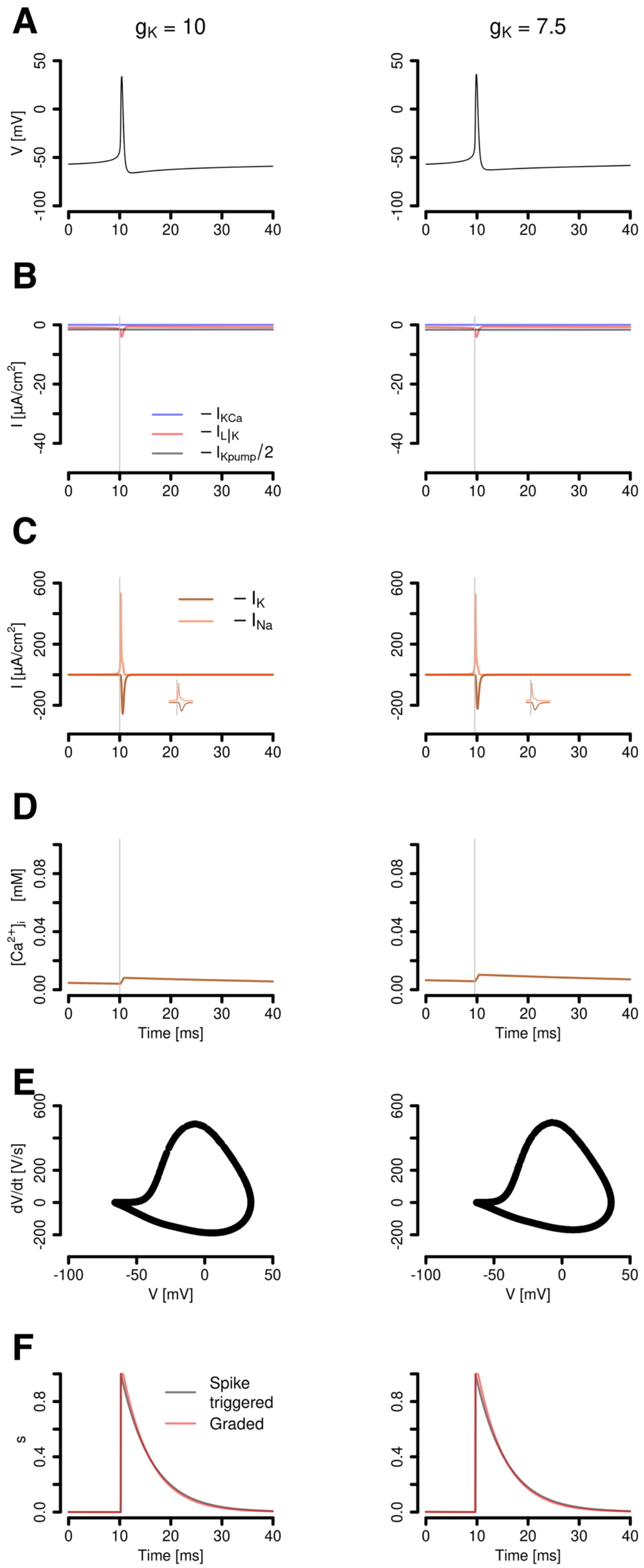

Figure 5. Effects of g_K downmodulation on ionic currents, intracellular calcium concentration $[Ca^{2+}]_i$, and synaptic properties during action potentials in the single FS inhibitory interneuron model. Same conventions as in Figure 3. More moderate effects on action potential broadening and other related variables are observed in comparison with the pyramidal neuron model.

inter-spike periods of highly suppressed activity, similar to what is commonly seen in some types of human focal seizures, specifically those characterized by ictal spike-wave discharges (Truccolo et al., 2011, 2014). These seizure-like dynamics were promoted by increasing $g_{syn}^{e\to e}$ and suppressed by larger $g_{syn}^{i\to e}$ synaptic couplings. As a concrete illustration, Figure 6*B–F*, corresponding to five increasing $g_{syn}^{e\to e}$ levels, respectively, show the gradual emergence of seizure-like dynamics in the form of recurrent and more and more synchronized neuronal-population spiking activity in the network.

In the following sections, we examine the effects of g_K downmodulation on network dynamics (Figs. 7, 8, 9), and how they compare to the reference network model, especially at the five chosen specific synaptic couplings for $g_{syn}^{e\to e}$ and $g_{syn}^{e\to e}$. Apart from the different g_K levels, all simulated networks share the same parameters. Overall, we will show that downmodulation of g_K can dramatically facilitate, via different synergistic effects, the emergence of seizure-like dynamics, even for cases of comparatively smaller $g_{syn}^{e\to e}$ synaptic levels that did not induce seizures in the base network model.

g_K downmodulation in the pyramidal neuron population leads to cascade of effects that promote metastability in network synchrony, lowering of seizure threshold, and prolonged seizure-like dynamics via graded synapses

Promotion of seizure-like network dynamics was observed in network simulations in which g_K was downmodulated even if only in the pyramidal neuron population. Figure 7 compares two network scenarios of g_K downmodulation in the pyramidal neuron population with the normal/reference network under normal g_K levels (Fig. 6). The two scenarios correspond to downmodulation of g_K of the pyramidal neuron population with and without the effects of broadened APs on effective synaptic coupling. For g_K without these effects, network simulations implemented synaptic interactions via spike-triggered synapses (Eq. 22). In the second scenario, the full cascade effects of g_K downmodulation were implemented, i.e., including graded synapses (Eq. 24). As discussed earlier (Materials and Methods), the duration and amplitude of action potentials can significantly and transiently affect the effective synaptic interaction/coupling between pre- and post-synaptic neurons. The motivation for doing the analysis separately in these two scenarios is to better discriminate the contributions of different mechanisms to the full cascade of effects initiated by g_K downmodulation.

The sample simulations show various degrees of emergence of synchronized network spiking activity in the pyramidal neuron population as g_K was downmodulated, irrespective of the inclusion of the effects of broadened APs (Fig. 7*A–F*). In particular, when compared to the reference network simulations (Fig. 6), g_K downmodulation without graded synapses was sufficient to promote, at low synaptic connectivity levels, the existence of a metastable regime where the network can switch back-and-forth between longer transients (>∼ 10 s) of low and high synchronization states in the spiking activity (e.g., Fig. 7*E*). This type of transitions was not observed with concomitant changes in glial state and $[K^+]_o$. Furthermore, substantial enhancement of network synchronization was observed when the full cascade effects of g_K downmodulation were included, easily inducing prolonged seizure-like dynamics (Fig. 7*C*,*F*).

Overall, g_k downmodulation in the pyramidal neuron population significantly reduced the synaptic connectivity threshold at which seizure-like dynamics could be induced. This seizure threshold was defined as the $g_{syn}^{e\to e}$ value at which the synchrony measure *S* of pyramidal neuron population crossed 0.3 (Materials and Methods). A reduction in this threshold value represents increased propensity of the network to exhibit prolonged synchronized

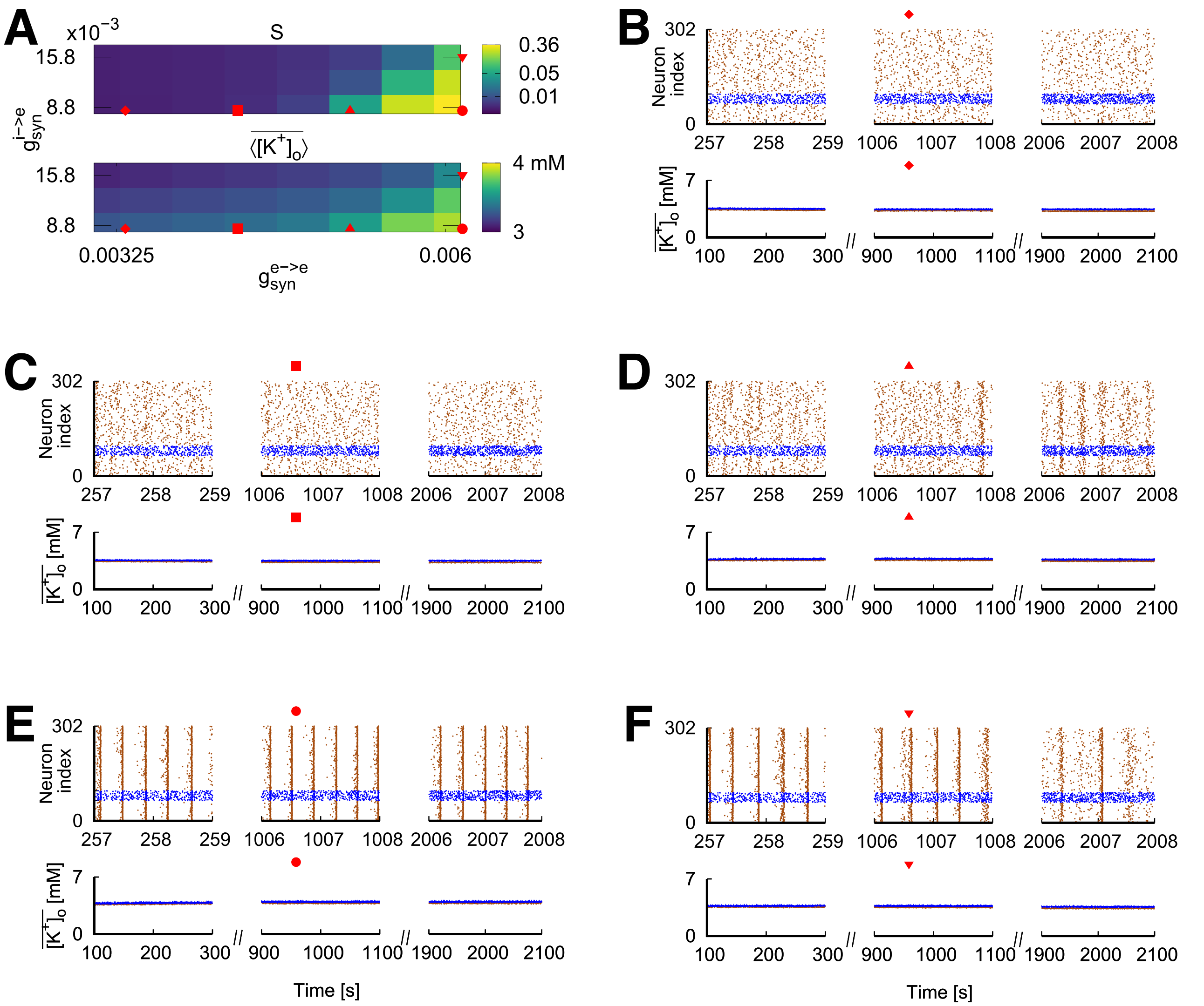

Figure 6. Reference cortical network dynamics under normal g_K conductances. Potassium conductance values were set to normal levels of $g_K = 15\,\mathrm{mS/cm^2}$ and $g_K = 10\,\mathrm{mS/cm^2}$ in the pyramidal neuron and fast-spiking inhibitory interneuron populations, respectively. Seizure-like activity emerges under appropriate excitatory and inhibitory synaptic coupling. ***A***, Heat map summaries of the synchrony measure (top panel) and mean $[K^+]_o$ of pyramidal cells (bottom panel) across all $g_{\mathrm{syn}}^{e\to e}$ and $g_{\mathrm{syn}}^{i\to e}$ values simulated. ***B–F***, Depiction of five simulation examples. The symbols in each example represent the synaptic strength values used for the particular simulation, with the matching symbols in panel ***A*** indicating the exact $g_{\mathrm{syn}}^{e\to e}$ and $g_{\mathrm{syn}}^{i\to e}$ values. Top panel: Three 2-second samples of spiking activity of every neuron in the network. Blue represents inhibitory interneurons and brown represents pyramidal neurons, respectively. Bottom panel shows the temporal progression of average $[K^+]_o$ for FS inhibitory interneuron (blue) and pyramidal cell (brown) sites. We note that while $g_{\mathrm{syn}}^{e\to e}$ increases from ***B-F***, ***F*** has a higher $g_{\mathrm{syn}}^{i\to e}$ synaptic coupling, resulting in slightly less synchronized neuronal-population spiking than in ***E***.

seizure-like dynamics. In the case when the effects of broadened APs were not included, downmodulation in the pyramidal neuron population from the normal case ($g_K = 15\,\mathrm{mS/cm^2}$) to $g_K = 0.3\,\mathrm{mS/cm^2}$ decreased the threshold value by $1.22 \pm 0.02 \times 10^{-3}\,\mathrm{mS/cm^2}$ (95% CI). Compared to the reference network, firing rates of both the pyramidal and FS interneuron populations at seizure threshold decreased in the g_K downmodulated case (Fig. 7*I,J*). As shown in the next subsection, this initial enhancement of network synchronization was the consequence of a cascade of effects arising from the change in intrinsic properties of the pyramidal neuron upon g_K downmodulation. As a consequence of the downstream effects, the basal network excitation and the overall stability landscape of the network changed, promoting the emergence of seizure-like dynamics.

The inclusion of the full effects of broadened APs via the use of graded synapses further reduced seizure thresholds by ($1.94 \pm 0.02 \times 10^{-3}\,\mathrm{mS/cm^2}$, 95% CI) as shown in Figure 7*G,H*. This additional reduction in seizure threshold was corroborated by the emergence of much more prolonged, sustained seizure-like dynamics (e.g., Fig. 7*F* vs Fig. 7*E*), and their occurrence over a wider range of $g_{\mathrm{syn}}^{e\to e}$ parameters than in g_K downmodulation without graded synapses (e.g., Fig. 7*C,F* vs Fig. 7*B,E*).

We emphasize that, in contrast to the spike-triggered synaptic variable (Eq. 22), which is only affected by spike timing, the duration and shape of an action potential (examined in detail in Figs. 3*A*, 5*A*) both have a considerable effect on the temporal progression of the graded synaptic variable (Eq. 24). In particular, broadened action potentials in pyramidal neurons can lead to sustained activation of the graded synaptic variable (Fig. 3*F*). Thus, given this new graded synaptic coupling, longer and larger action potentials should lead to longer and larger excitatory post-synaptic potentials (EPSPs) in the network. (We also note that, although present, the effect was much less noticeable in the FS inhibitory

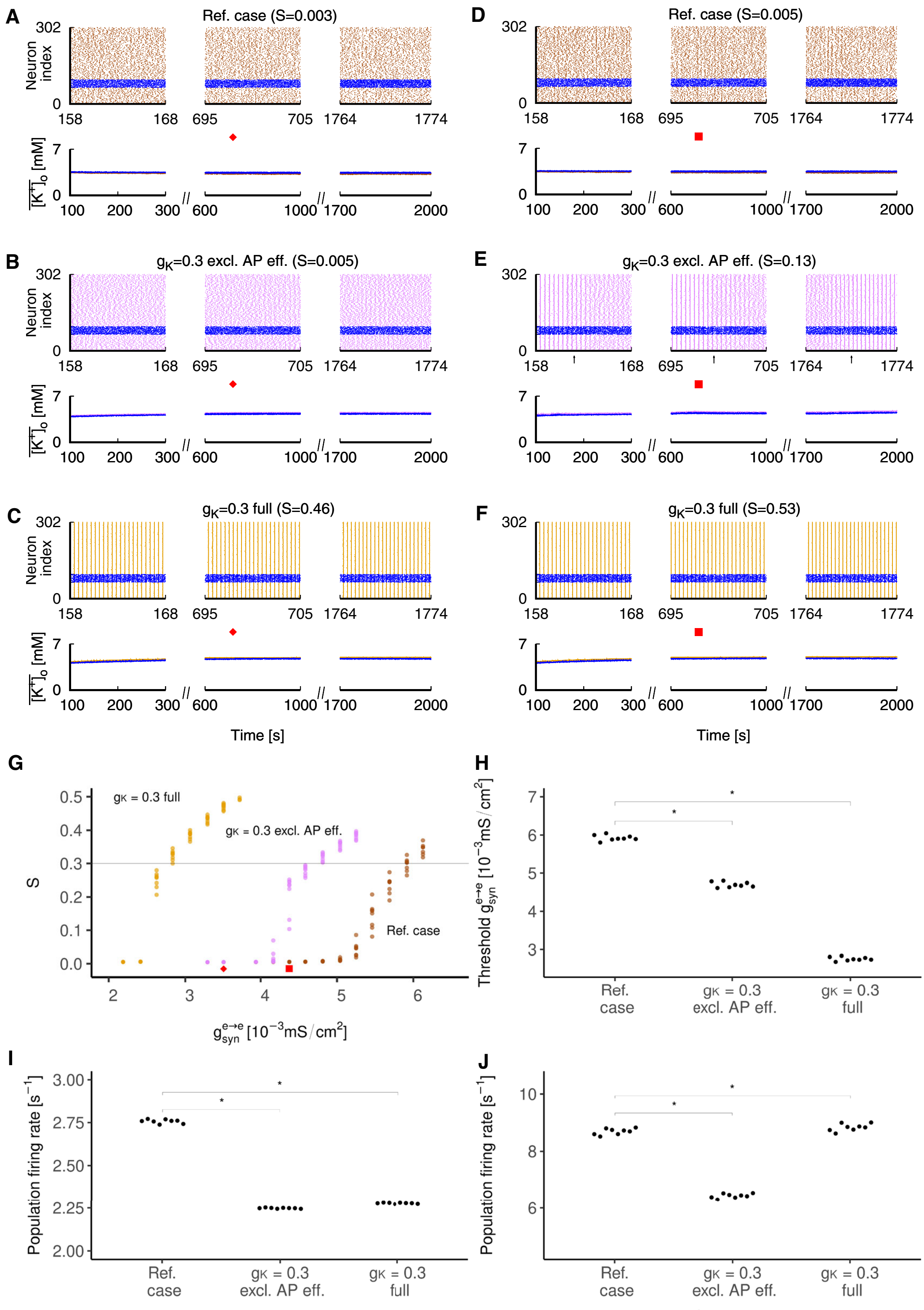

Figure 7. Cortical network dynamics: effects of g_K downmodulation in pyramidal neurons. The left (***A,B,C***) and right (***D,E,F***) columns compare the effects of g_K downmodulation with respect to a normal/reference network under *very weak* (diamond) and *weak* (square) excitatory-excitatory connectivity or synaptic coupling strengths, respectively. These two synaptic coupling strengths correspond to regimes where the synchrony measure in the reference network is near zero ($S \approx 0$). The actual connectivity (for both $g_{syn}^{e \to e}$ and $g_{syn}^{i \to e}$) values are indicated by the position of the icons in (***G***) and Figure 6*A*. ***A,D***, Activity of reference cortical networks under very weak (***A***) and weak (***D***) synaptic connectivity. ***B,C***, Two different g_K downmodulation scenarios are examined: one without graded synapses (i.e., without the action potential broadening effect on synaptic coupling; denoted by "excl. AP eff."; shown in ***B***), and another with it (denoted by "full," shown in ***C***). In this very weak $g_{syn}^{e \to e}$ synaptic coupling, emergence of seizure-like activity requires the full cascade of g_K downmodulation effects, i.e., graded synapses that capture the effect of action potential broadening. ***E,F***, In the weak $g_{syn}^{e \to e}$ synaptic coupling regime, where the reference network (***D***) starts to show only sparse and very short synchronized activity transients, either of the two g_K downmodulation scenarios is sufficient to elicit seizure-like activity, as clearly indicated by the higher synchrony measures S. Moreover, although in

interneuron model (Fig. 5*F*), primarily due to the chosen level for g_K downmodulation.)

We also note that, in this study, the time constants τ_e and τ_i (Table 2) for the graded synaptic variables (Eq. 24) were normalized against their spike-triggered counterparts (Eq. 22), so that the time-integrated synaptic variable per spike in either the spike-triggered or graded case were approximately equal to each other in the reference/normal g_K level (Figs. 3*F*, 5*F*). The purpose of normalizing $\tau_{\{e,i\}}$ at the single neuron level was to allow for a better evaluation of the net effects of graded synapses on network activities (Fig. 7*C*,*F*) as compared to the reference/base case (Fig. 6) and to the case in which effects of broadened APs were excluded (i.e., simulations implemented with spike-triggered synapses–Fig. 7*B*,*E*).

In sum, g_K downmodulation can lead to emergent seizure-like dynamics via various synergistic mechanisms, including the less direct transient effects of broadened of action potentials on the synaptic dynamics between pyramidal neurons. The resulting longer and larger action potentials can lead to larger and longer lasting EPSPs, thus transiently increasing the effective synaptic coupling and excitability in the simulated cortical networks. This increased excitability further facilitates the emergence of seizure-like dynamics.

Shifted rheobases and increased I_{KCa}s of pyramidal neurons upon g_K downmodulation can enhance synchronized neuronal spiking in network dynamics

At the single neuron level, g_K downmodulation of pyramidal neurons can lead to 1) a notable shift in rheobase (Fig. 2*C*), and 2) a drastic increase in Ca^{2+} mediated potassium currents I_{KCa} (Fig. 3*B*). The slower acting I_{KCa} as compared to the faster I_K lengthens the inter-spike intervals, and subsequently alters the overall f-I characteristics of the neuron (Fig. 2*C*). In this subsection, we examined whether and how these changes at the single neuron level were associated to the observed g_K enhancement of network synchronization (Fig. 7*E*). Additional sets of network simulations were performed here. These simulations involved manipulation of different conductance and current parameters to create scenarios in which single neuronal mechanisms were isolated, such that their effects on network dynamics could be studied independently. We focused on effects of the components of g_K downmodulation mechanisms not directly associated with broadened APs. Thus, we revert to the use of spike-triggered synapses (Eq. 22) on all network simulations.

We start by examining how network simulations, under different g_K downmodulation levels, transition into synchronized network dynamics as the connectivity/synaptic coupling $g_{\mathrm{syn}}^{e\to e}$ is varied (Fig. 8*A*). The analysis shows that g_K downmodulation in pyramidal neurons (mauve curve in 8*A*) enhances the synchronization measure *S* for significantly lower $g_{\mathrm{syn}}^{e\to e}$ values than in the normal g_K case (brown curve in 8*A*). Specifically, the synchronization enhancement of network dynamics upon g_K downmodulation showed both (1) a sharper/steeper and (2) an earlier increase in the synchrony measure *S* with increasing $g_{\mathrm{syn}}^{e\to e}$. These effects can be examined in more detail in terms of rheobase shifts and the role of I_{KCa}.

First, to understand the effect of a shifted rheobase on the g_K downmodulated network, we compensated the effects of the shifted rheobase by injecting a constant hyperpolarizing current to the g_K downmodulated pyramidal neuron population (black curve, Fig. 8*A*). The magnitude of the hyperpolarizing current was the same as the amount of the rheobase shift at the single neuron level. The resulting network exhibited a delayed start of rise in the synchrony measure *S*, yet maintained a similar steepness of rising as the original g_K downmodulated network (mauve curve), indicating that a shifted rheobase at the single neuron level was primarily associated with a start of transition into synchronous dynamics at a smaller $g_{\mathrm{syn}}^{e\to e}$ of the g_K downmodulated network.

Second, in a different set of network simulations, we directly increased I_{KCa} by artificially increasing the calcium mediated potassium conductance value g_{KCa} of the pyramidal neurons. A direct increase in g_{KCa} singles out I_{KCa} and its roles in the neuron's f-I characteristics while bypassing other g_K downmodulation effects on the pyramidal neuron including broadening of action potentials and effects on I_{Na}. Thus, the setup allowed for considering the effects of I_{KCa} on network dynamics in isolation.

The network simulations upon this direct increase in g_{KCa} and also a constant depolarizing current, both applied to the pyramidal neuron population, largely replicated the network dynamics of the original g_K downmodulated simulations. In particular, the network simulations (mustard green curve and spike plots in Fig. 8*A*,*B*) matched both the increased rate of increase in the synchronization measure *S* and also the transition point at which *S* began to rise of the original g_K downmodulated simulations (mauve curve and spike plots in Fig. 8*A*,*B*). Considering that the association between the shifted rheobase at the single neuron level and the $g_{\mathrm{syn}}^{e\to e}$ value at which *S* started to rise was already previously established, we have thus demonstrated here that the increased I_{KCa} at the single neuron level was primarily associated with a steeper transition into synchrony (i.e., a higher rate of rise in *S*), of the g_K downmodulated network.

Finally, to further understand how an increase in I_{KCa} could lead to a steeper increase in synchronization as the network transitioned into seizure-like dynamics, we performed current pulse perturbation analyses (similar to phase resetting curves; Materials and Methods) on both normal g_K and g_K downmodulated single pyramidal neuron models. The objective of the analyses was to assess the sensitivity of the neurons during periodic spiking to external current perturbations. The results of the analyses (Fig. 8*C*–*E*) demonstrated increased robustness of the almost periodic spiking of the g_K downmodulated pyramidal neuron model against perturbations. At the network level, increased robustness of this almost periodic

←

(***E***) the network can transition back-and-forth between transients of low and high synchronization states (i.e., network metastability; transition points indicated by the arrows), the full cascade of g_K downmodulation effects, including graded synapses, results in sustained seizure-like synchronized activity as shown in (***F***). ***G***,***H***, Either g_K downmodulation with or without graded synapses in pyramidal neurons can induce seizure-like activity at much lower $g_{\mathrm{syn}}^{e\to e}$ synaptic coupling levels than in the reference/normal network case. For comparison (***G***), while the reference case requires a coupling $g_{\mathrm{syn}}^{e\to e} \sim 6\times10^{-3}$ mS/cm^2 to reach a synchronization level S=0.3 (Materials and Methods), the full g_K downmodulation cascade effects can lead to the same synchrony level under a much weaker coupling $g_{\mathrm{syn}}^{e\to e} \sim 3\times10^{-3}$ mS/cm^2. In (***H***), the statistical testing confirms the above findings. (Eight sets of stochastic simulations, indicated as dots, where each simulation had different random seeds for synaptic connectivity instantiations and synaptic background noises, were used. Here, as also in (***I***,***J***) below, the Wilcoxon signed-rank test was used Wilcoxon, 1945). Statistical significance at p =0.0078 is indicated by the symbol *. ***I***, Comparison between pyramidal neuron population firing rates at threshold $g_{\mathrm{syn}}^{e\to e}$ (i.e., point at which S=0.3 in (G)) for each of the two g_K downmodulation scenarios and the reference network case. Identical simulations as in **G**,**H** were used here. ***J***, Comparison between firing rates of the inhibitory interneuron population at threshold $g_{\mathrm{syn}}^{e\to e}$ for each of the two g_K downmodulation scenarios. Identical simulations as in **G**,**H** were used here. In addition, in all of the above network simulations, $g_{\mathrm{syn}}^{i\to e} = 0.0088\,\mathrm{mS/cm^2}$.

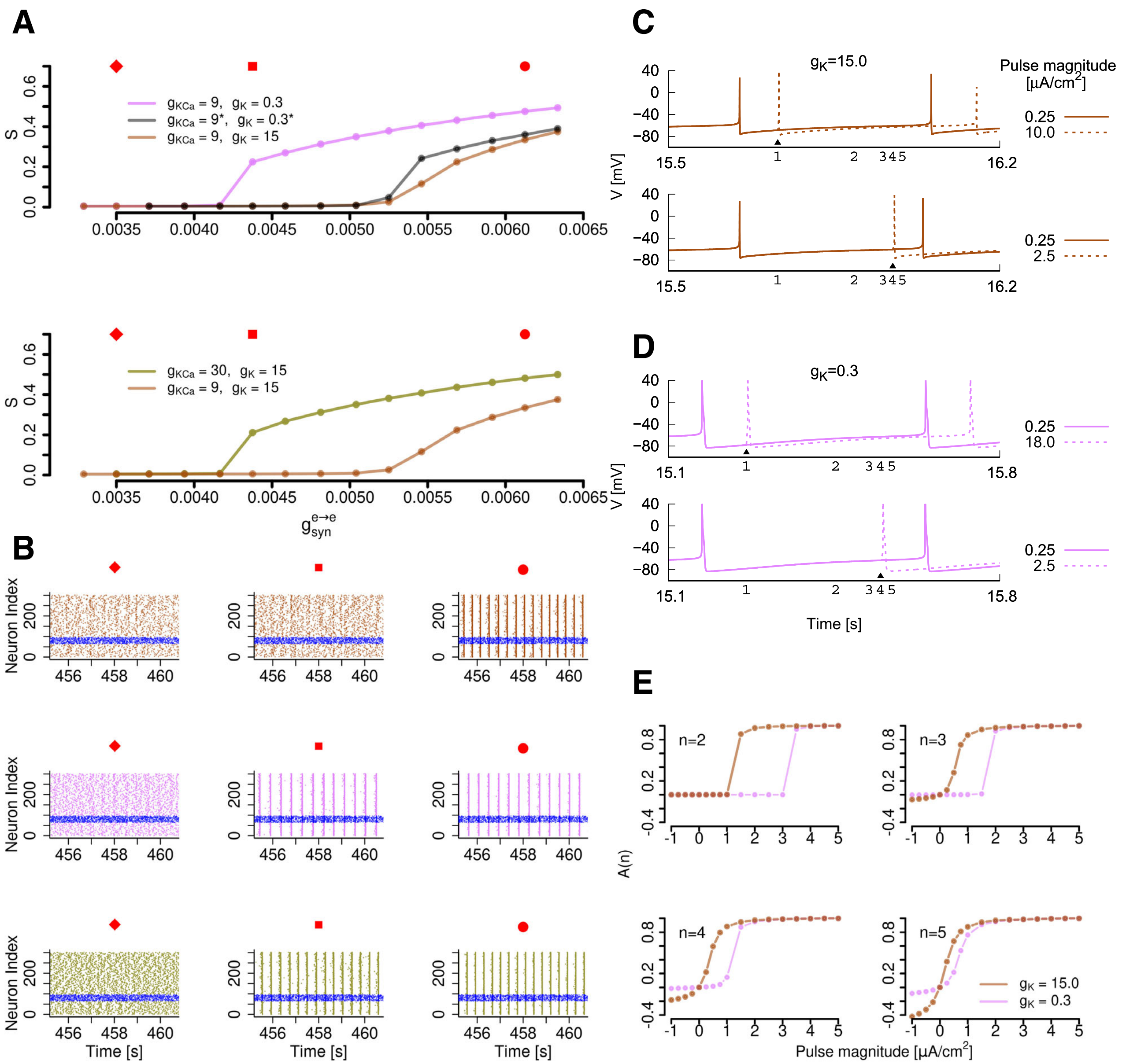

Figure 8. Mechanisms underlying enhancement of network synchronization by g_K downmodulation in pyramidal neurons. Overall, reduction in g_K leads to both a shift in rheobase and an increase in I_{KCa}. The combination of these two effects contributes to network synchronization and the emergence of recurrent (almost periodic) epileptic-like neuronal-population spiking dynamics at lower $g_{syn}^{e \to e}$ levels than in the base network model. In addition, via a pulse perturbation approach (akin to phase response curve analysis), we show that g_K downmodulation in pyramidal neurons, via the increased I_{KCa}, makes their spiking activity more robust to noise perturbations in this almost periodic regime, thus favoring synchronization across the network. In every network simulation of this figure, $g_{syn}^{i \to e} = 0.0088\ \mathrm{mS/cm^2}$. ***A*** Top panel: synchrony index vs synaptic coupling strength $g_{syn}^{e \to e}$ obtained from 3 sets of network simulations representing three different g_{KCa} and g_K conditions. For $g_K = 0.3\ \mathrm{mS/cm^2}$, the synchronization index (mauve curve) starts to deviate from zero at a lower $g_{syn}^{e \to e}$ ($\sim 0.0042\ \mathrm{mS/cm^2}$) and with a steeper slope than in the normal g_K case (brown). Since g_K downmodulation can shift the rheobase, as seen earlier in Figure 2*C*, the effects observed here could have directly resulted from just a rheobase shift. To control for this possibility, we ran another set of simulations with the same $g_K = 0.3\ \mathrm{mS/cm^2}$ downmodulation level, but now with an extra constant hyperpolarizing current of 0.11 $\mu\mathrm{A/cm^2}$ applied to the pyramidal population to compensate for the rheobase shift. Under this new condition, the synchronization index curve (black) deviates from zero at a higher $g_{syn}^{e \to e}$, but still with a similar curvature to the original $g_K = 0.3\ \mathrm{mS/cm^2}$ case without rheobase compensation. Thus, a rheobase shift only partially explains the difference in network synchrony between pyramidal populations with a normal and downmodulated g_K values. In particular, a rheobase shift does not account for the more abrupt transition into synchronized activity of the g_K downmodulated pyramidal population, as compared to the normal g_K case. We hypothesized that, as well as a rheobase shift, an increase in I_{KCa} was also required. This increase in I_{KCa} was shown earlier for the single-neuron model, Figure 3*B*, as a consequence of g_K downmodulation. Bottom panel: To test this hypothesis, g_K was kept at a normal level while g_{KCa} was significantly increased to 30 mS/cm² (mustard-green curve), such that there was a direct increase in I_{KCa} comparable in magnitude but without the action potential broadening effects associated with a decrease in g_K. An extra 0.11 µA/cm² constant *depolarizing* current was also applied to the pyramidal population to make the rheobase identical to the original g_K downmodulated case (i.e., mauve curve in the top panel). As seen in the plot, an increase in g_{KCa} led to enhanced synchronization with approximately the same curvature as in the top panel for $g_K = 0.3\ \mathrm{mS/cm^2}$. Thus, to achieve both the early and steeper increase in synchrony, both a shift in rheobase and an increase in I_{KCa} are required, respectively. The mauve, black and mustard-green curves are essentially the same curves, except for a translation along the $g_{syn}^{e \to e}$ axis, but the brown curve cannot be made equivalent to any of the three curves with this translation, showing that an increased I_{KCa} is primarily associated with a steeper transition into network synchronization. Furthermore, in both the top and bottom panels, this enhanced synchronization effect is restricted to $g_{syn}^{e \to e}$ values at which transition into network synchronization is occurring. For higher $g_{syn}^{e \to e}$ values, the rate of increase in synchrony with respect to $g_{syn}^{e \to e}$ is higher in the normal g_K level than in the reduced g_K level. ***B***, Network dynamics (spike raster plots) corresponding to three of the conditions examined in ***A*** as indicated by the different coloring of the pyramidal neuron spikes. Different $g_{syn}^{e \to e}$ levels are indicated by the geometric icons. The same effects examined in ***A*** are very clearly seen in the earlier emergence of synchronized (almost periodic) seizure-like spiking activity in the pyramidal population

spiking state translates into increased stability of periodic synchronized network dynamics once they are formed.

In summary, our analyses of this section showed that both an increase in I_{KCa} and a shifted rheobase of pyramidal cells were primarily required, respectively, for a sharper and at a smaller $g_{syn}^{e\to e}$ transition into seizure-like dynamics (Fig. 8*A*,*B*). In particular, a current pulse perturbation analysis (akin to a phase response curve analysis; Fig. 8*C*–*E*) showed that once a pyramidal neuron was in an almost periodic spiking regime, g_K downmodulation made the spiking dynamics much more robust to noise perturbations, which would otherwise disrupt the neuron's periodic spiking and the stability of the synchronized activity across the network.

While moderate g_K downmodulation in the FS inhibitory interneuron population can suppress short synchronization transients, strong downmodulation leads to depolarization block in the population and abrupt emergence of seizure-like dynamics

Next, we examined the effects of moderate g_K downmodulation on the dynamics of the cortical network model when the downmodulation was restricted to FS inhibitory interneurons (Fig. 9). Two levels of g_K downmodulation representing moderate and strong were considered here. In the case of moderate g_K downmodulation, we set $g_K = 7.0\,\mathrm{mS/cm^2}$ while keeping g_K for the pyramidal neurons the same value as in the base or reference network. In the case of strong g_K downmodulation, g_K of FS inhibitory interneurons was initially kept at a normal level, but was gradually reduced to $0.03\,\mathrm{mS/cm^2} \sim 480\,\mathrm{s}$ into the simulation.

Comparing the reference/normal case simulation sample with the g_K=7.0 mS/cm^2 revealed a slight decrease in the synchrony of the pyramidal neuron population as a result of moderate g_K downmodulation of FS inhibitory interneurons (Fig. 9*B*). Moderate g_K downmodulation increased the firing rates of FS inhibitory interneurons (for comparison, see Figs. 4*C*, 9*H*). The increased inhibition marginally lowered the pyramidal neuron population firing rate (Fig. 9*G*). Consequently, a higher $g_{syn}^{e\to e}$ threshold as compared to the reference case was required for seizure-like dynamics to occur (an increase of $0.30 \pm 0.02 \times 10^{-3}$ mS/cm^2, 95% CI–Fig. 9*F*).

In contrast to the moderate g_K reduction, a strong g_K downmodulation in the FS inhibitory interneuron population, while keeping g_K normal in the pyramidal neuron population, resulted in dramatic promotion of seizure-like dynamics (Fig. 9*C*,*G*). Notably, the transition into a seizure is preceded by a fast (1–2 s) and large transient increase in the firing rate of the FS inhibitory interneuron population (Fig. 9*D*). Just before seizure onset, this increase then fastly collapsed to a very low level activity (Fig. 9*D*,*H*) accompanied simultaneously by a large increase in extracellular potassium concentration, especially for interstitial and extracellular spaces near FS inhibitory interneurons. In the pyramidal neuron population, this fast seizure onset is characterized by the immediate transition into recurrent almost periodic and synchronized neuronal population spiking activity.

This early reduction in inhibitory spiking activity, accompanied by increased potassium concentrations, eventually evolved into full depolarization block and cessation of inhibition in the network. At this point, all the recurrent, almost-periodic and highly synchronized neuronal-population spiking activity was primarily maintained by the activity in the pyramidal neuron population. Overall, the cessation of inhibition as a result of depolarization block of FS interneurons led to a considerable decrease in seizure threshold as compared to the reference case (a decrease of $0.78{\pm}0.03 \times 10^{-3}$ mS/cm^2, 95% CI–Fig. 9*F*).

The above results also point to the specificity of depolarization block events to FS inhibitory interneurons in our network model simulations. This higher sensitivity of FS inhibitory interneurons has been explored in previous studies, e.g., Ho and Truccolo (2016) among others. In a different context, Lemaire et al. (2021) have also argued for the specificity of depolarization block in FS inhibitory neurons in computational and slice models of genetic pediatric seizures (Na$_V$1.1/SCN1A mutation leading to abnormal extracellular potassium concentrations), while depolarization block in both pyramidal neurons and FS inhibitory interneurons would instead lead to migraine-like cortical spreading depolarization.

Discussion

We have shed new light on how voltage-gated potassium conductances contribute to shaping single-neuron spiking activity and neuronal network dynamics by systematically examining neocortical network models built upon conductance-based single-compartment neurons. Our simulations were motivated by recent results from animal models of focal epilepsy (Avoli et al., 1996; Žiburkus et al., 2006; Librizzi et al., 2017; Wenzel et al., 2017, 2019; Scalmani et al., 2023) and therapeutic interventions based on modulation of potassium channels for epilepsy, multiple sclerosis and spinal-cord injury (Dietrich et al., 2021; Paredes-Cruz et al., 2022; Qiu et al., 2022). While these results

←

(mauve and mustard-green). ***C***, Single-neuron pulse perturbation analysis. Simulations in both the upper and lower panels are the same as in Figure 2*A* (normal g_K level), except now an additional pulse perturbation is given at one of the time locations, indicated by the numbers 1 to 5, during the inter-spike interval. These five time points partition the inter-spike interval of the unperturbed neuron at the 20, 60, 75, 80 and 85 percentage marks. The top panel shows an example for a brief (3 ms) pulse current perturbation at time location 1 (as indicated by the triangle). Minimal or a minor perturbation of the timing of the succeeding action potential results when the magnitude of the injected current pulse is small, as exemplified by the solid membrane potential traces in both panels. However, a sufficiently large current pulse results in a larger temporal advance or delay of the succeeding action potential, as indicated by the dashed membrane potential traces. A measure was developed ($A(n)$, Eq. 29) to assess how sensitive the single-neuron dynamics was to pulse perturbation at those five time locations during the interspike interval. Briefly, a measure of value 0 indicates no perturbation effect, i.e., subsequent spikes are not advanced nor delayed, and 1 corresponds to the extreme case where an action potential is almost immediately elicited by the perturbation. For instance, the value of this measure at time point 4 (bottom panel), $A(4)$, for the solid membrane potential trace is 0.3, in agreement with the observation that the pulse perturbation advances the spike occurrence, but not almost immediately. ***D***, Single-pulse perturbations analysis. Simulations in both the upper and lower panels originate from Figure 2*B* (reduced g_K). In this example, the values of the measure for the dashed membrane potential traces in both panels (time points 1 and 4) are both close to 1, in agreement with the fact that a spike was almost immediately elicited by the current pulse perturbation. ***E***, Sensitivity of the single-neuron spiking dynamics to current pulse perturbations of different magnitudes and at different time locations during the inter-spike interval (n = 3, 4, 5 and 6), for normal g_K = 15 and reduced $g_K = 0.3\,\mathrm{mS/cm^2}$. The same measure (Eq. 29) described above for the sensitivity of AP (action potential) time to pulse perturbations is used here. g_K downmodulation makes the spiking dynamics significantly less sensitive to pulse perturbations, as evidenced by the higher current threshold of eliciting any AP advance or delay, and the lower uncertainty in the timing of elicited APs of the pyramidal neuron with a reduced $g_K = 0.3\,\mathrm{mS/cm^2}$. Based on this observation, one concludes that within a network simulation, increase in I_{KCa} being a consequence of g_K downmodulation makes the spiking dynamics more robust to noise perturbations, which is associated with a steeper increase in S during transition. These perturbations would otherwise jitter spike times way from a synchronized regime. Summarizing, the combined analyses from (***A***,***B***) and pulse perturbation assessments (***C***–***E***) indicate that g_K downmodulation in pyramidal neurons enhances network synchrony by both shifting the rheobase and increasing I_{KCa}, and eventually making synchronized network spiking dynamics more robust against weaker $g_{syn}^{e\to e}$ values and de-synchronizing noise perturbations.

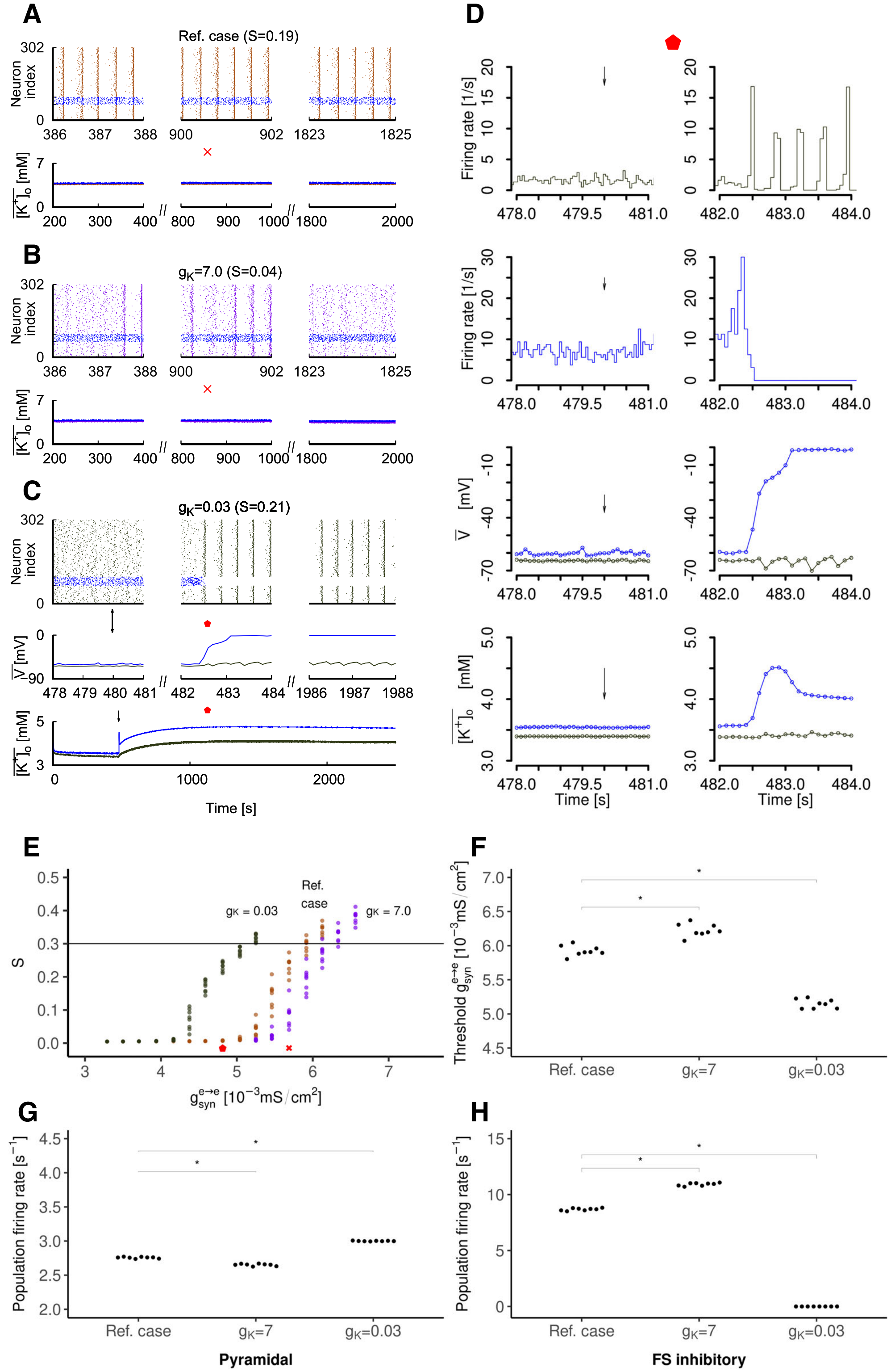

Figure 9. Cortical network dynamics: effects of g_K downmodulation in the FS inhibitory interneuron population. ***A,B***, In comparison to reference (normal) network activity under shown in (***A***), moderate $g_K = 7.0\,\mathrm{mS/cm^2}$ downmodulation in the fast-spiking inhibitory interneuron population (***B***) can actually suppress some of the sychronization transients under the same synaptic coupling parameters. The synaptic coupling, equal in (***A***) and (***B***), is denoted by the red cross icon (see (***E***) for the actual $g_{syn}^{e\rightarrow e}$ value), and the pyramidal neuron population had normal $g_K = 15\,\mathrm{mS/cm^2}$. ***C***, In contrast, strong $g_K = 0.03\,\mathrm{mS/cm^2}$ downmodulation in FS inhibitory interneurons led to dramatic effects including depolarization block of these interneurons and prolonged seizure-like dynamics. We note also that this can happen even for a much weaker synaptic coupling level (indicated by the red pentagon icon) where the reference/normal the synchrony measure in the network is near zero (S≈ 0; see (***E***)). To better visualize the time course of this severe g_K downmodulation, the potassium conductance was kept at a normal level ($g_K = 10\,\mathrm{mS/cm^2}$) until time $t = 480$ s (see arrow). After that, g_K decreased linearly to reach $0.03\,\mathrm{mS/cm^2}$ at $t = 483$ s. This terminal level of g_K was maintained until the end of simulations. Meanwhile, the pyramidal neuron population had normal $g_K = 15\,\mathrm{mS/cm^2}$ throughout the simulation. Cessation of spiking in the inhibitory population (starting soon after downmodulation, at

have pointed out to the importance of potassium conductances and related ionic concentrations to epileptic network dynamics and therapeutic interventions, untangling the complex relationship between ion channels within individual neurons, and further in terms of the emerging network dynamics, remains a major challenge. Therefore, systematic computational modeling and simulation approaches play a crucial role into providing a coherent picture of all the complexities involved and in generating new experimental predictions.

Overall, our findings show how g_K downmodulation in pyramidal neurons and FS inhibitory interneurons can lead to a series of downstream effects, starting with the broadening of action potentials due to interaction of various ionic currents, and the ensuing enhancement of the robustness to noise perturbations during periodic spiking regimes, and effects on synaptic coupling. In addition, g_K downmodulation can lead to differential effects on excitatory and FS inhibitory neurons, contributing to depolarization block in the latter under relatively high levels of downmodulation. In the majority of g_K downmodulation scenarios that we examined, all these changes act synergistically to enhance network synchronization, especially for the pyramidal neuron population, thus creating pathways to the emergence of seizure-like dynamics. This seizure activity was characterized by almost-periodic neuronal-population spiking activity. In addition, our findings indicate how, under appropriate levels, g_k downmodulation can also play a therapeutic role in other neurological disorders by improving communication in neuronal circuits and networks as a result of the broadened action potentials" effects.

The observed g_K downmodulation effect leading to enhanced network synchronization in the pyramidal neuron population (Fig. 7) is the downstream consequence of both a lowered rheobase and an increased I_{KCa} of the pyramidal neurons (Fig. 8). It should be emphasized, however, that the specific combination of mechanisms that enables both an earlier (i.e., with a smaller $g_{\mathrm{syn}}^{e\rightarrow e}$ connectivity strength) and a steeper transition into network synchronization depends on the choice of a "non-epileptic" state as the initial condition in our network simulations. Our choice of background synaptic parameters (Eq. 26) fixes the reference "non-epileptic" network state as the one in which firing activities in both the pyramidal and FS inhibitory interneuron populations are just above their rheobases. We think that this choice for the reference "non-epileptic" state is reasonable, given that the lower firing rates of both excitatory and inhibitory populations are representative of many normal physiological brain states.

The seemingly paradoxical results of network synchronization enhancement despite the I_{KCa} suppressive effects on the neuronal firing rates (Fig. 7) can be understood as follows. g_K downmodulation leads to two mechanisms with opposing effects on the tonic firing rates of pyramidal neurons under noisy synaptic background inputs: (a) an increase in I_{KCa} which strengthens spike frequency adaptation and decreases the tonic firing rates (Brenner et al., 2005), and (b) a lower rheobase which promotes the neuron's basal excitability and thus increases its firing rates. However, the relative effects on the tonic firing rates of these two mechanisms are dependent upon the original (i.e., normal g_K) firing rates of the neuron. In the regime where the original neurons are firing close to rheobase, a lowered rheobase provides a larger I_{ext} range for the noisy neuron to produce a spike, but the increased I_{KCa} only minimally decreases the tonic firing rate within a restricted I_{ext} range. The combined effects of these two mechanisms still result in comparable net tonic firing rates between the g_K downmodulated and normal g_K neurons over the entire dynamic range of background synaptic inputs. Furthermore, while previous computational studies have shown diverse mechanisms and noise effects on the synchronization in neuronal networks (McMillen and Kopell, 2003; Ho et al., 2012, 2014; Meng and Riecke, 2018; Zirkle and Rubchinsky, 2021; Rebscher et al., 2022), the steeper increase in network synchronization of the pyramidal population observed here is associated with a more robust resistance against noise perturbations arising from the stronger I_{KCa} in the g_K downmodulated pyramidal neurons (Fig. 8*A*,*C*,*E*).

Our study was motivated in part by 4-AP acute models of focal seizures and our findings contribute to the understanding of how 4-AP administration leads to seizures via all the revealed synergistic effects of g_k downmodulation. One might argue that the relevance of 4-AP seizure models might be very limited, especially to the case of pharmacologically resistant epilepsy since 4-AP animal models appear to respond well to standard anti-epileptic medication (Heuzeroth et al., 2019). On the other hand, several other studies indicate that K-channelopathies, and related disruptions in g_K functioning, are likely common in idiopathic and pharmacologically-resistant epilepsies (D'Adamo et al., 2013; Köhling and Wolfart, 2016), thus supporting the broader relevance of our study. Our predicted synergistic effects of g_K downmodulation might be tested in 4-AP in vivo and slice preparations, and with more systematic and localized manipulations of g_K conductances in different types of neuronal populations. Our finding that pyramidal excitatory neurons and FS inhibitory interneurons can respond very differently to different 4-AP levels might also help explain previously observed dose-dependent effects of 4-AP administration in animal models of focal seizures (Myers et al., 2018).

We have directly examined the effects of g_K downmodulation only in neuronal somata. An important open problem is the detailed computational modeling and examination of g_k downmodulation in dendrites, axons and presynaptic sites. For example, experimental evidence points to gK downmodulation effects on signal propagation in dendritic trees (Johnston et al., 2000; Kim and Hoffman, 2008; Hoffman, 2013). Another important

←

about 482.5 s) is associated with its strong membrane depolarization as shown in the middle plot. The temporal resolution of average membrane potentials is 100 ms. ***D***, To examine in more detail the transition into the seizure-like neuronal spiking activity, the following zoomed-in plots show the firing rates for both pyramidal neuron (dark green) and FS inhibitory interneuron (blue) populations (two top rows, respectively), and the mean membrane potential and $\overline{[K^+]_o}$ values (two bottom rows), around the seizure transition time in ***C***. The temporal resolution of spike counts is 50 ms. The downmodulation onset time is indicated by the arrows at 480 s. Interestingly, soon after g_K reduction, there is a fast and large transient increase in the firing rate of the FS inhibitory interneuron population, followed by an increase in extracellular potassium concentration near this population. Its spiking rate then collapses to virtually zero, and is then accompanied by the fast transition of the pyramidal neuron population activity into recurrent almost periodic firing. ***E,F***, Strong g_K downmodulation in the FS inhibitory interneuron population can lead to seizure-like dynamics (e.g., synchronization levels of $S = 0.3$) at significantly lower $g_{\mathrm{syn}}^{e\rightarrow e}$ values than in the reference ("Ref. case") network. Also, as expected from (***B***), the profile for the moderate g_K downmodulation and for the reference network cases are about the same. In these and following plots, the same conventions and statistical tests as in Figure 7*G*,*H* were used. ***G***, Comparison between pyramidal neuron population firing rates at threshold $g_{\mathrm{syn}}^{e\rightarrow e}$ (i.e., point at which $S = 0.3$ in (***E***)) for the moderate and strong g_K downmodulation regimes and the reference network case. ***H***, Comparison between firing rates of the FS inhibitory interneuron population at threshold $g_{\mathrm{syn}}^{e\rightarrow e}$ for the moderate and strong g_K downmodulation regimes and the reference network case. Same simulation data as in E,F were used in (***G,H***). In all of the above network simulations, $g_{\mathrm{syn}}^{i\rightarrow e} = 0.0088\ \mathrm{mS/cm^2}$.

open issue is the assessment of the contribution of gap junctions and corresponding syncytia in (parvalbumin-positive) FS inhibitory interneurons (Papasavvas et al., 2020) to seizure-like dynamics under g_K downmodulation. We have also not systematically investigated how g_K downmodulation might interact with several other hypothesized ways through which activated inhibitory interneuron populations might contribute to seizure initiation and maintenance (Librizzi et al., 2017; Magloire et al., 2019; Dudok et al., 2021; Gentiletti et al., 2022; Scalmani et al., 2023). These include, among others, exhaustion of inhibition (Trevelyan et al., 2006; Zhang et al., 2012; Ho and Truccolo, 2016), post-inhibitory rebounds of pyramidal neurons (Sessolo et al., 2015; Assaf and Schiller, 2016; Rich et al., 2020b), and GABA-driven depolarization effects due to shifts in GABA reversal potential resulting from Cl^- loading (Cohen et al., 2002; Timofeev et al., 2002; Krishnan and Bazhenov, 2011; Lillis et al., 2012).

In addition, González et al. (2018) have shown in biophysical network models under 4-AP that transient synchronized GABAergic-interneuron activity (simulated via external inputs) can lead to seizures via a cascade of effects starting with $[Cl^-]_i$ increase in excitatory neurons, followed by the activation of their K^+-Cl^- co-transporter KCC2, thus resulting in both Cl^- and K^+ efflux, and finally high enough $[K^+]_o$ depolarizing levels to trigger a seizure onset. (See also Moore et al., 2018; Dzhala and Staley, 2021; Gentiletti et al., 2022 for other perspectives on the role of KCC2 in seizures.) In contrast, we note that in our model, 4-AP-induced g_K downmodulation can intrinsically lead (i.e., without the need of external inputs) to transient firing rate increases in the FS inhibitory population before the transition to seizure-like activity in the network (Fig. 9*G*). Furthermore, even during these transient increases, the firing rates in the FS inhibitory population remain relatively low (<30 spikes/s) such that GABA-driven $[Cl^-]_i$ levels in pyramidal neurons would not be high enough to substantially increase KCC2 activation. Therefore, we do not think that the introduction of KCC2 dynamics in our model would have changed the main findings of this study.

Finally, we note that we have focused on the case of seizures that evolve into and are dominated by ictal spike-wave discharges. The case of low-voltage fast-activity seizures is likely to have a much more preserved and important role for FS inhibitory interneurons, as we Ho and Truccolo (2016), Truccolo et al. (2011, 2014), and Wagner et al. (2015) and others (Uva et al., 2015; Librizzi et al., 2017; Elahian et al., 2018; Dossi and Huberfeld, 2023) have proposed. Another important issue is how g_k downmodulation might relate to fluctuations in brain excitability at the many different time scales, from circadian to multiday rhythms, as shown in recent studies (Proix et al., 2021), and to the spatiotemporal seizure spreading dynamics in large-scale brain networks (Proix et al., 2018; Moosavi et al., 2022; Moosavi and Truccolo, 2023). We hope to address the above issues in future studies.

Data and Code Availability Statement

All the data and codes used for the simulations of single-neuron and cortical network models can be accessed via either MODELDB https://modeldb.science/2018263 or via the Brown repository https://doi.org/10.26300/1evm-8w31.

References

Abbott LF, Marder E (1998) Modeling small networks. In: *Methods in neuronal modeling* (Koch C, Segev I, eds), pp 361–410. Cambridge, MA: MIT Press.

Alviña K, Khodakhah K (2010) The therapeutic mode of action of 4-aminopyridine in cerebellar ataxia. J Neurosci 30:7258–7268.

Anderson WS, Kudela P, Cho J, Bergey GK, Franaszczuk PJ (2007) Studies of stimulus parameters for seizure disruption using neural network simulations. Biol Cybern 97:173–194.

Assaf F, Schiller Y (2016) The antiepileptic and ictogenic effects of optogenetic neurostimulation of PV-expressing interneurons. J Neurophysiol 116:1694–1704.

Avoli M, Barbarosie M, Lücke A, Nagao T, Lopantsev V, Köhling R (1996) Synchronous GABA-mediated potentials and epileptiform discharges in the rat limbic system in vitro. J Neurosci 16:3912–3924.

Barish ME, Ichikawa M, Tominaga T, Matsumoto G, Iijima T (1996) Enhanced fast synaptic transmission and a delayed depolarization induced by transient potassium current blockade in rat hippocampal slice as studied by optical recording. J Neurosci 16:5672–5687.

Bates D, Maechler M (2021) *Matrix: sparse and dense matrix classes and methods*. https://CRAN.R-project.org/package=Matrix. R package version 1.3-3.

Bazhenov M, Timofeev I, Steriade M, Sejnowski TJ (2004) Potassium model for slow (2–3 hz) in vivo neocortical paroxysmal oscillations. J Neurophysiol 92:1116–1132.

Bean B (2007) The action potential in mammalian central neurons. Nat Rev Neurosci 8:451–465.

Beswick-Jones H, Hopper AJ, Brown AM (2023) Activity-dependent fluctuations in interstitial [k+]: investigations using ion-sensitive microelectrodes. Molecules 28:523.

Bostock H, Sears T, Sherratt R (1981) The effects of 4-aminopyridine and tetraethylammonium ions on normal and demyelinated mammalian nerve fibres. J Physiol 313:301–315.

Brenner R, Chen QH, Vilaythong A, Toney GM, Noebels JL, Aldrich RW (2005) Bk channel β4 subunit reduces dentate gyrus excitability and protects against temporal lobe seizures. Nat Neurosci 8:1752–1759.

Buchin A, Chizhov A, Huberfeld G, Miles R, Gutkin BS (2016) Reduced efficacy of the KCC2 cotransporter promotes epileptic oscillations in a subiculum network model. J Neurosci 36:11619–11633.

Carnevale NT, Hines ML (2006) *The neuron book*. Cambridge, UK: Cambridge University Press.

Chao OY, Yang Y-M (2019) Timing constraints of action potential evoked Ca2+ current and transmitter release at a central nerve terminal. Sci Rep 9:4448.

Cohen I, Navarro V, Clemenceau S, Baulac M, Miles R (2002) On the origin of interictal activity in human temporal lobe epilepsy in vitro. Science 298: 1418–1421.

Cressman JR, Ullah G, Ziburkus J, Schiff SJ, Barreto E (2009) The influence of sodium and potassium dynamics on excitability, seizures, and the stability of persistent states: I. Single neuron dynamics. J Comput Neurosci 26:159–170.

D'Adamo MC, Catacuzzeno L, Di Giovanni G, Franciolini F, Pessia M (2013) K+ channelepsy: progress in the neurobiology of potassium channels and epilepsy. Front Cell Neurosci 7:134.

Destexhe A, Mainen ZF, Sejnowski TJ (1994) An efficient method for computing synaptic conductances based on a kinetic model of receptor binding. Neural Comput 6:14–18.

Dietrich M, Hartung H-P, Albrecht P (2021) Neuroprotective properties of 4-aminopyridine. Neurol - Neuroimmunol Neuroinflammation 8:e976.

Dossi E, Huberfeld G (2023) Gabaergic circuits drive focal seizures. Neurobiol Dis 180:106102.

Dudok B, Klein PM, Soltesz I (2021) Toward understanding the diverse roles of perisomatic interneurons in epilepsy. Epilepsy Curr 22:54–60.

Dura-Bernal S, et al. (2019) NetPyNE, a tool for data-driven multiscale modeling of brain circuits. eLife 8:e44494.

Dzhala VI, Staley KJ (2021) Kcc2 chloride transport contributes to the termination of ictal epileptiform activity. Eneuro 8:ENEURO.0208-20.2020.

Elahian B, et al. (2018) Low-voltage fast seizures in humans begin with increased interneuron firing. Ann Neurol 84:588–600.

Ermentrout B (2002) *Simulating, analyzing, and animating dynamical systems: a guide to XPPAUT for researchers and students*. Society for Industrial and Applied Mathematics (SIAM), Philadelphia. Available at: https://epubs.siam.org/doi/pdf/10.1137/1.9780898718195.fm

Frankenhaeuser B, Hodgkin AL (1956) The after-effects of impulses in the giant nerve fibres of Loligo. J Physiol 131:341–376.

Fröhlich F, Bazhenov M, Iragui-Madoz V, Sejnowski TJ (2008) Potassium dynamics in the epileptic cortex: new insights on an old topic. Neuroscientist 14:422–433.

Fröhlich F, Sejnowski TJ, Bazhenov M (2010) Network bistability mediates spontaneous transitions between normal and pathological brain states. J Neurosci 30:10734–10743.

Gentiletti D, de Curtis M, Gnatkovsky V, Suffczynski P (2022) Focal seizures are organized by feedback between neural activity and ion concentration changes. Elife 11:e68541.

Golomb D, Rinzel J (1993) Dynamics of globally coupled inhibitory neurons with heterogeneity. Phys Rev E Stat Phys Plasmas Fluids Relat Interdiscip Topics 48:4810–4814.

Golomb D, Rinzel J (1994) Clustering in globally coupled inhibitory neurons. Physica D 72:259–282.

Golomb D, Wang XJ, Rinzel J (1994) Synchronization properties of spindle oscillations in a thalamic reticular nucleus model. J Neurophysiol 72: 1109–1126.

González OC, Shiri Z, Krishnan GP, Myers TL, Williams S, Avoli M, Bazhenov M (2018) Role of KCC2-dependent potassium efflux in 4-aminopyridine-induced epileptiform synchronization. Neurobiol Dis 109:137–147.

Hedrich UB, et al. (2021) 4-aminopyridine is a promising treatment option for patients with gain-of-function kcna2-encephalopathy. Sci Transl Med 13:eaaz4957.

Hester J, Wickham H, Bryan J (2022) *vroom: read and write rectangular text data quickly*. https://CRAN.R-project.org/package=vroom. R package version 1.6.0.

Heuzeroth H, Wawra M, Fidzinski P, Dag R, Holtkamp M (2019) The 4-aminopyridine model of acute seizures in vitro elucidates efficacy of new antiepileptic drugs. Front Neurosci 13:677.

Hijazi S, Smit AB, van Kesteren RE (2023) Fast-spiking parvalbumin-positive interneurons in brain physiology and Alzheimer's disease. Mol Psychiatry 28:4954–4967.

Hines M, Carnevale T (2014) NEURON simulation environment. In: *Encyclopedia of computational neuroscience* (Jaeger D, Jung R, eds), pp 1–8. New York, NY: Springer.

Ho ECY, Eubanks JH, Zhang L, Skinner FK (2014) Network models predict that reduced excitatory fluctuations can give rise to hippocampal Network hyper-excitability in meCP2-null mice. PLoS One 9:e91148.

Ho ECY, Strüber M, Bartos M, Zhang L, Skinner FK (2012) Inhibitory networks of fast-spiking interneurons generate slow population activities due to excitatory fluctuations and network multistability. J Neurosci 32: 9931–9946.

Ho ECY, Truccolo W (2016) Interaction between synaptic inhibition and glial-potassium dynamics leads to diverse seizure transition modes in biophysical models of human focal seizures. J Comput Neurosci 41: 225–244.

Hoffman DA (2013) K+ channel regulation of multicompartmental signal integration. Neuron 79:403–405.

Izhikevich EM (2007) *Dynamical systems in neuroscience: the geometry of excitability and bursting*. Cambridge, MA: MIT Press.

Johnston D, Hoffman DA, Poolos NP (2000) Potassium channels and dendritic function in hippocampal pyramidal neurons. Epilepsia 41:1072–1073.

Kaczmarek L, Zhang Y (2017) Kv3 channels: enablers of rapid firing, neurotransmitter release, and neuronal endurance. Physiol Rev 97:1431–1468.

Kager H, Wadman WJ, Somjen GG (2000) Simulated seizures and spreading depression in a neuron model incorporating interstitial space and ion concentrations. J Neurophysiol 84:495–512.

Kelley C, Newton AJH, Hrabetova S, McDougal RA, Lytton WW (2022) Multiscale computer modeling of spreading depolarization in brain slices. eNeuro 9:ENEURO.0082-22.2022.

Kelley D, Richards C (2024) *oce: analysis of oceanographic data*. https://dankelley.github.io/oce/. R package version 1.8-3.

Kim J, Hoffman DA (2008) Potassium channels: newly found players in synaptic plasticity. Neuroscientist 14:276–286.

Köhling R, Wolfart J (2016) Potassium channels in epilepsy. Cold Spring Harb Perspectives Med 6:a022871.

Krishnan GP, Bazhenov M (2011) Ionic dynamics mediate spontaneous termination of seizures and postictal depression state. J Neurosci 31:8870–8882.

Krishnan GP, Filatov G, Bazhenov M (2013) Dynamics of high-frequency synchronization during seizures. J Neurophysiol 109:2423–2437.

Lemaire L, Desroches M, Krupa M, Pizzamiglio L, Scalmani P, Mantegazza M (2021) Modeling nav1. 1/scn1a sodiumchannelmutations in amicrocircuit with realistic ion concentration dynamics suggests differential gabaergic mechanisms leading to hyperexcitability in epilepsy and hemiplegic migraine. PLoS Comput Biol 17:e1009239.

Librizzi L, Losi G, Marcon I, Sessolo M, Scalmani P, Carmignoto G, Curtis MD (2017) Interneuronal network activity at the onset of seizure-like events in entorhinal cortex slices. J Neurosci 37:10398–10407.

Lien C-C, Jonas P (2003) Kv3 potassium conductance is necessary and kinetically optimized for high-frequency action potential generation in hippocampal interneurons. J Neurosci 23:2058–2068.

Lillis KP, Kramer MA, Mertz J, Staley KJ, White JA (2012) Pyramidal cells accumulate chloride at seizure onset. Neurobiol Dis 47:358–366.

Locke RE, Nerbonne JM (1997a) Role of voltage-gated k+ currents in mediating the regular-spiking phenotype of callosal-projecting rat visual cortical neurons. J Neurophysiol 78:2321–2335.

Locke RE, Nerbonne JM (1997b) Three kinetically distinct Ca2+-independent depolarization-activated k+ currents in callosal-projecting rat visual cortical neurons. J Neurophysiol 78:2309–2320.

Magloire V, Mercier MS, Kullmann DM, Pavlov I (2019) GABAergic interneurons in seizures: investigating causality with optogenetics. Neuroscientist 25:344–358.

McDougal R, Hines M, Lytton W (2013) Reaction-diffusion in the neuron simulator. Front Neuroinformatics 7:28.

McKinney W (2010) Data structures for statistical computing in python. In: *Proceedings of the 9th python in science conference* (van der Walt S, Millman J, eds), pp 56–61. SciPy 2010, Austin, Texas.

McMillen D, Kopell N (2003) Noise-stabilized long-distance synchronization in populations of model neurons. J Comput Neurosci 15:143–157.

Meng JH, Riecke H (2018) Synchronization by uncorrelated noise: interacting rhythms in interconnected oscillator networks. Sci Rep 8:6949.

Mitterdorfer J, Bean BP (2002) Potassium currents during the action potential of hippocampal CA3 neurons. J Neurosci 22:10106–10115.

Mochida S (2022) Mechanisms of synaptic vesicle exo- and endocytosis. Biomedicines 10:1593.

Moore YE, Deeb TZ, Chadchankar H, Brandon NJ, Moss SJ (2018) Potentiating kcc2 activity is sufficient to limit the onset and severity of seizures. Proc Natl Acad Sci 115:10166–10171.

Moosavi SA, Jirsa VK, Truccolo W (2022) Critical dynamics in the spread of focal epileptic seizures: network connectivity, neural excitability and phase transitions. PLoS One 17:e0272902.

Moosavi SA, Truccolo W (2023) Criticality in probabilistic models of spreading dynamics in brain networks: epileptic seizures. PLoS Comput Biol 19: e1010852.

Myers TL, Gonzalez OC, Stein JB, Bazhenov M (2018) Characterizing concentration-dependent neural dynamics of 4-aminopyridine-induced epileptiform activity. Epilepsy J 4:128.

Newton AJH, McDougal RA, Hines ML, Lytton WW (2018) Using neuron for reaction-diffusion modeling of extracellular dynamics. Front Neuroinform 12:41.

Papasavvas CA, Parrish RR, Trevelyan AJ (2020) Propagating activity in neocortex, mediated by gap junctions and modulated by extracellular potassium. Eneuro 7:ENEURO.0387-19.2020.

Paredes-Cruz M, Grijalva I, Martínez-López YE, Guizar-Sahagún G, Colín-Ramírez E, Rojano-Mejía D (2022) Functional improvement in individuals with chronic spinal cord injury treated with 4-aminopyridine: a systematic review. Front Neurol 13:1034730.

Perucca P, Dubeau F, Gotman J (2013) Intracranial electroencephalographic seizure-onset patterns: effect of underlying pathology. Brain 137:183–196.

Proix T, Jirsa VK, Bartolomei F, Guye M, Truccolo W (2018) Predicting the spatiotemporal diversity of seizure propagation and termination in human focal epilepsy. Nat Commun 9:1–15.

Proix T, Truccolo W, Leguia MG, Tcheng TK, King-Stephens D, Rao VR, Baud MO (2021) Forecasting seizure risk in adults with focal epilepsy: a development and validation study. Lancet Neurol 20:127–135.

Qiu Y, et al. (2022) On-demand cell-autonomous gene therapy for brain circuit disorders. Science 378:523–532.

R Core Team (2022) *R: a language and environment for statistical computing*. R Foundation for Statistical Computing, Vienna, Austria. https://www.R-project.org/

Rebscher L, Obermayer K, Metzner C (2022) Synchronization through uncorrelated noise in excitatory-inhibitory networks. Front Comput Neurosci 16:825865.

Rich S, Chameh HM, Rafiee M, Ferguson K, Skinner FK, Valiante TA (2020b) Inhibitory network bistability explains increased interneuronal activity prior to seizure onset. Front Neural Circuits 13:81.

Rich S, Zochowski M, Booth V (2020a) Effects of neuromodulation on excitatory–inhibitory neural network dynamics depend on network connectivity structure. J Nonlinear Sci 30:2171–2194.

Scalmani P, Paterra R, Mantegazza M, Avoli M, Curtis MD (2023) Involvement of GABAergic interneuron subtypes in 4-aminopyridine-induced seizure-like events in mouse entorhinal cortex in vitro. J Neurosci 43:1987–2001.

Scarnati MS, Clarke SG, Pang ZP, Paradiso KG (2020) Presynaptic calcium channel open probability and changes in calcium influx throughout the action potential determined using AP-waveforms. Front Synaptic Neurosci 12:17.

Sessolo M, Marcon I, Bovetti S, Losi G, Cammarota M, Ratto GM, Fellin T, Carmignoto G (2015) Parvalbumin-positive inhibitory interneurons oppose propagation but favor generation of focal epileptiform activity. J Neurosci 35:9544–9557.

Sharp AA, Skinner FK, Marder E (1996) Mechanisms of oscillation in dynamic clamp constructed two-cell half-center circuits. J Neurophysiol 76:867–883.

Sherratt RM, Bostock H, Sears TA (1980) Effects of 4-aminopyridine on normal and demyelinated mammalian nerve fibres. Nature 283:570–572.

Skinner FK (2006) Conductance-based models. Scholarpedia 1:1408. revision #125663.

Smart SL, Lopantsev V, Zhang C, Robbins CA, Wang H, Chiu S, Schwartzkroin PA, Messing A, Tempel BL (1998) Deletion of the kv1. 1 potassium channel causes epilepsy in mice. Neuron 20:809–819.

Somjen GG (2002) Ion regulation in the brain: implications for pathophysiology. Neuroscientist 8:254–267.

Somjen GG, Kager H, Wadman WJ (2008) Computer simulations of neuron-glia interactions mediated by ion flux. J Comput Neurosci 25:349–365.

Thier SO (1986) Potassium physiology. Am J Med 80:3–7.

Timofeev I, Grenier F, Bazhenov M, Sejnowski TJ, Steriade M (2000) Origin of slow cortical oscillations in deafferented cortical slabs. Cereb Cortex 10: 1185–1199.

Timofeev I, Grenier F, Steriade M (2002) The role of chloride-dependent inhibition and the activity of fast-spiking neurons during cortical spike–wave electrographic seizures. Neuroscience 114:1115–1132.

Traub RD, Colling SB, Jefferys J (1995) Cellular mechanisms of 4-aminopyridine-induced synchronized after-discharges in the rat hippocampal slice. J Physiol 489:127–140.

Traub RD, Contreras D, Cunningham MO, Murray H, LeBeau FEN, Roopun A, Bibbig A, Wilent WB, Higley MJ, Whittington MA (2005) Single-column thalamocortical network model exhibiting gamma oscillations, sleep spindles, and epileptogenic bursts. J Neurophysiol 93:2194–2232.

Trevelyan AJ, Sussillo D, Watson BO, Yuste R (2006) Modular propagation of epileptiform activity: evidence for an inhibitory veto in neocortex. J Neurosci 26:12447–12455.

Truccolo W, Ahmed OJ, Harrison MT, Eskandar EN, Cosgrove GR, Madsen JR, Blum AS, Potter NS, Hochberg LR, Cash SS (2014) Neuronal ensemble synchrony during human focal seizures. J Neurosci 34:9927–9944.

Truccolo W, Donoghue JA, Hochberg LR, Eskandar EN, Madsen JR, Anderson WS, Brown EN, Halgren E, Cash SS (2011) Single-neuron dynamics in human focal epilepsy. Nat Neurosci 14:635–641.

Ullah G, Cressman JR, Barreto E, Schiff SJ (2009) The influence of sodium and potassium dynamics on excitability, seizures, and the stability of persistent states. II. Network and glial dynamics. J Comput Neurosci 26:171–183.

Ushey K, Allaire J, Tang Y (2021) *reticulate: interface to 'Python'*. https://CRAN.R-project.org/package=reticulate. R package version 1.22.

Uva L, Breschi GL, Gnatkovsky V, Taverna S, de Curtis M (2015) Synchronous inhibitory potentials precede seizure-like events in acute models of focal limbic seizures. J Neurosci 35:3048–3055.

Wagner FB, Eskandar EN, Cosgrove GR, Madsen JR, Blum AS, Potter NS, Hochberg LR, Cash SS, Truccolo W (2015) Microscale spatiotemporal dynamics during neocortical propagation of human focal seizures. Neuroimage 122:114–130.

Wang XJ, Buzsáki G (1996) Gamma oscillation by synaptic inhibition in a hippocampal interneuronal network model. J Neurosci 16:6402–6413.

Wei Y, Ullah G, Ingram J, Schiff SJ (2014a) Oxygen and seizure dynamics: II. Computational modeling. J Neurophysiol 112:213–223.

Wei Y, Ullah G, Schiff S (2014b) Unification of neuronal spikes, seizures, and spreading depression. J Neurosci 34:11733–11743.

Wenzel M, Hamm JP, Peterka DS, Yuste R (2017) Reliable and elastic propagation of cortical seizures in vivo. Cell Rep 19:2681–2693.

Wenzel M, Hamm JP, Peterka DS, Yuste R (2019) Acute focal seizures start as local synchronizations of neuronal ensembles. J Neurosci 39:8562–8575.

Wheeler DB, Randall A, Tsien RW (1996) Changes in action potential duration alter reliance of excitatory synaptic transmission on multiple types of ca2+ channels in rat hippocampus. J Neurosci 16:2226–2237.

Wickham H (2016) *ggplot2: elegant graphics for data analysis*. New York: Springer-Verlag. https://ggplot2.tidyverse.org

Wickham H, François R, Henry L, Müller K (2022) *dplyr: a grammar of data manipulation*. https://CRAN.R-project.org/package=dplyr. R package version 1.0.10.

Wilcoxon F (1945) Individual comparisons by ranking methods. Biometrics Bull 1:80–83.

Williams T, Kelley C (2020) Gnuplot 5.4: an interactive plotting program. http://gnuplot.sourceforge.net/

Yang Y-M, Wang L-Y (2006) Amplitude and kinetics of action potential-evoked ca2+ current and its efficacy in triggering transmitter release at the developing calyx of held synapse. J Neurosci 26:5698–5708.

Yuan W, Burkhalter A, Nerbonne JM (2005) Functional role of the fast transient outward k+ current ia in pyramidal neurons in (rat) primary visual cortex. J Neurosci 25:9185–9194.

Zhang ZJ, Koifman J, Shin DS, Ye H, Florez CM, Zhang L, Valiante TA, Carlen PL (2012) Transition to seizure: ictal discharge is preceded by exhausted presynaptic GABA release in the hippocampal CA3 region. J Neurosci 32:2499–2512.

Žiburkus J, Cressman JR, Barreto E, Schiff SJ (2006) Interneuron and pyramidal cell interplay during in vitro seizure-like events. J Neurophysiol 95: 3948–3954.

Zirkle J, Rubchinsky LL (2021) Noise effect on the temporal patterns of neural synchrony. Neural Netw 141:30–39.